UPPSALA
UNIVERSITET

Digital Comprehensive Summaries of Uppsala Dissertations from the Faculty of Science and Technology 136

Band Alignment Between ZnO-Based and $Cu(In,Ga)Se_2$ Thin Films for High Efficiency Solar Cells

CHARLOTTE PLATZER-BJÖRKMAN

ACTA
UNIVERSITATIS
UPSALIENSIS
UPPSALA
2006

ISSN 1651-6214
ISBN 91-554-6435-1
urn:nbn:se:uu:diva-6263

Dissertation presented at Uppsala University to be publicly examined in Häggsalen, Ångströmslaboratoriet, Uppsala, Friday, February 3, 2006 at 09:30 for the degree of Doctor of Philosophy. The examination will be conducted in English.

Abstract

Platzer-Björkman, C. 2006. Band Alignment Between ZnO-Based and Cu(In,Ga)Se_2 Thin Films for High Efficiency Solar Cells. Acta Universitatis Upsaliensis. *Digital Comprehensive Summaries of Uppsala Dissertations from the Faculty of Science and Technology* 136. 80 pp. Uppsala. ISBN 91-554-6435-1.

Thin-film solar cells based on Cu(In,Ga)Se_2 contain a thin buffer layer of CdS in their standard configuration. In order to avoid cadmium in the device for environmental reasons, Cd-free alternatives are investigated. In this thesis, ZnO-based films, containing Mg or S, grown by atomic layer deposition (ALD), are shown to be viable alternatives to CdS.

The CdS is an n-type semiconductor, which together with the n-type ZnO top-contact layers form the pn-junction with the p-type Cu(In,Ga)Se_2. From device modeling it is known that a buffer layer conduction band (CB) position of 0-0.4 eV above that of the Cu(In,Ga)Se_2 layer is consistent with high photovoltaic performance. For the Cu(In,Ga)Se_2/ZnO interface this position is measured by photoelectron spectroscopy and optical methods to –0.2 eV, resulting in increased interface recombination. By including sulfur into ZnO, a favorable CB position to Cu(In,Ga)Se_2 can be obtained for appropriate sulfur contents, and device efficiencies of up to 16.4% are demonstrated in this work. From theoretical calculations and photoelectron spectroscopy measurements, the shift in the valence and conduction bands of Zn(O,S) are shown to be non-linear with respect to the sulfur content, resulting in a large band gap bowing.

ALD is a suitable technique for buffer layer deposition since conformal coverage can be obtained even for very thin films and at low deposition temperatures. However, deposition of Zn(O,S) is shown to deviate from an ideal ALD process with much larger sulfur content in the films than expected from the precursor pulsing ratios and with a clear increase of sulfur towards the Cu(In,Ga)Se_2 layer.

For (Zn,Mg)O, single-phase ZnO-type films are obtained for Mg/(Zn+Mg) < 0.2. In this region, the band gap increases almost linearly with the Mg content resulting in an improved CB alignment at the heterojunction interface with Cu(In,Ga)Se_2 and high device efficiencies of up to 14.1%.

Keywords: solar cells, Cu(In Ga)Se2, atomic layer deposition, ZnO, Zn(O S), (Zn Mg)O, band alignment, photoelectron spectroscopy

Charlotte Platzer-Björkman, Department of Engineering Sciences, Solid State Electronics, Box 534, Uppsala University, SE-75121 Uppsala, Sweden

ISSN 1651-6214
ISBN 91-554-6435-1
urn:nbn:se:uu:diva-6263 (http://urn.kb.se/resolve?urn=urn:nbn:se:uu:diva-6263)

Till min familj

List of publications

This thesis is based on the following publications, which will be referred to in the text by their Roman numerals.

I J.Sterner, C. Platzer-Björkman and L. Stolt, **"XPS/UPS monitoring of ALCVD ZnO growth on Cu(In,Ga)Se_2 absorbers"**, in: Proceedings of the 17th European Photovoltaic Solar Energy Conference (WIP-Renewable Energies, Munich, 2001) **II** p. 1118-21

II C. Platzer-Björkman, J. Lu, J. Kessler and L.Stolt, **"Interface study of $CuInSe_2$/ZnO and Cu(In,Ga)Se_2/ZnO devices using ALD ZnO buffer layers"**, Thin Solid Films **431-432** (2003) p. 321-325

III C. Platzer-Björkman, J. Kessler and L. Stolt, **"Analysis of Zn(O,S) films for Cu(In,Ga)Se_2 solar cells"**, Proceedings of the Estonian Academy of Sciences Physics Mathematics, **52**(3) (2003) p. 299-307

IV C. Platzer-Björkman, J. Kessler and L. Stolt, **"Atomic Layer Deposition of Zn(O,S) buffer layers for high efficiency Cu(In,Ga) Se_2 solar cells"**, in: Proceedings of the 3rd World Conference on Photovoltaic Energy Conversion (WCPEC-3 Organizing Committee, Osaka, 2003) **1** p. 461-464

V C. Platzer-Björkman, T. Törndahl, J. Kessler and L. Stolt, **"Reproducibility of CIGS based solar cells with ALD Zn(O,S) buffer layers"**, to appear in Proceedings of the 20th European Photovoltaic Solar Energy Conference 2005

VI C. Persson, C. Platzer-Björkman, J. Malmström, T. Törndahl and M. Edoff, **"Strong valence-band offset bowing of $ZnO_{1-x}S_x$ enhances p-type nitrogen doping of ZnO-like alloys"**, Submitted

VII C. Platzer-Björkman, T. Törndahl, D. Abou-Ras, J. Malmström, J. Kessler, and L. Stolt, **"Zn(O,S)/Cu(In,Ga)Se_2 solar cells: band alignment and sulfur gradient"**, Submitted

VIII T. Törndahl, C. Platzer-Björkman, J. Kessler and M. Edoff, **"Atomic Layer Deposition of $Zn_{1-x}Mg_xO$ buffer layers for $Cu(In,Ga)Se_2$ solar cells"**, Submitted

Comments on my contributions

I Part of the experimental work and writing

II All experimental work except TEM, writing with input from co-authors

III All experimental work, writing with input from co-authors

IV All experimental work, writing with input from co-authors

V All experimental work except XRD analysis, writing with input from co-authors

VI Contributions to the definition of the project, sample preparation, UPS/XPS analysis, part of the writing

VII All experimental work except optical analysis, TEM and XRD work, writing with input from co-authors

VIII Contributions to the definition of the project, part of device preparation, analysis and optical analysis, part of the writing

Related work not included in the thesis

I M. Igalson and C. Platzer-Björkman, **"The influence of buffer layer on the transient behaviour of thin film chalcopyrite devices"**, Solar Energy Materials and Solar Cells **84** (2004) p. 93-103

II U. Malm, J. Malmström, C. Platzer-Björkman and L. Stolt, **"Determination of dominant recombination paths in Cu(In,Ga)Se_2 thin-film solar cells with ALD-ZnO buffer layers"**, Thin Solid Films **480-481** (2005) p. 208-212

Contents

1. Introduction

The interest in renewable energy production is increasing. Reports on global warming from greenhouse gas emission, rising oil prices and a steadily rising demand for electricity in developing countries clearly show a need for new solutions. Several renewable technologies are being developed and the common challenge for these new and often technically advanced technologies is to reach cost-competitiveness relative to the established non-renewable energy production. Governmental subsidies, and taxes on non-renewable energy production are supporting the renewable technologies in many countries. However, the opinion on how much clean energy may cost will probably vary over time depending on the economical wealth and environmental awareness. To obtain a complete transfer of the energy production to renewable technologies both reduction of the cost of the renewable energy and acceptance for including the cost of pollution into the price for non-renewable energy are needed. Cost reduction of the electricity produced by solar cells is the main motivation for the development of thin film solar cells. This thesis is a part of that development, with the additional objective of making efficient thin film solar cells that do not contain hazardous materials.

1.1 Solar cells

Solar cells convert the energy in sunlight directly into electricity. For this, two basic functions are required: absorption of the sunlight and charge separation of the electron-hole pairs that are created. The photoelectric effect, observed in the 1880's and explained later by Einstein, is the transfer of the energy in light (photon energy) to the absorbing material through excitation of electrons. Most solar cells are made of solid semiconductor materials, the most common being silicon, Si. The history of solar cells can be found in Ref. [1] and the physics and operational principles of solar cells in Ref. [2].

Solar cells produce electricity only when light shines on them. For practical use, energy storage of some kind is needed. For isolated solar systems electrochemical batteries or mechanical storage such as flywheels or water pumping can be used. Connection of solar cells to the electricity grid is another option. One example is grid connected domestic systems, where solar modules on the roof of a house deliver electricity to the household. During overproduction, the excess electricity is fed into the grid. Reversibly, if the

solar modules cannot supply all electricity needed, the grid acts as a backup. For this to work, part of the grid-connected electricity generation must be able to compensate for the variation in the solar generated power.

The solar cell market has grown rapidly over the last 5-10 years, mainly due to subsidy programs in Japan, Germany and some other countries. The price of solar modules and system components has decreased but not yet to the level where solar electricity can compete with conventional power production. However, there are niche-markets where solar power is competitive such as space-applications and isolated houses. The solar cell market is dominated by crystalline silicon. Larger production volumes and advances in the technology may still lower the price of silicon solar modules, but not down to a competitive price, which is about 1/2 to 1/10 of the price today [1]. Thin film solar cells, with much lower material consumption and simplified production, have a greater potential to reach that goal.

1.2 Thin film solar cells based on $Cu(In,Ga)Se_2$

The structure of a thin film solar cell based on $Cu(In,Ga)Se_2$ (called CIGS) is shown in fig 1.1.

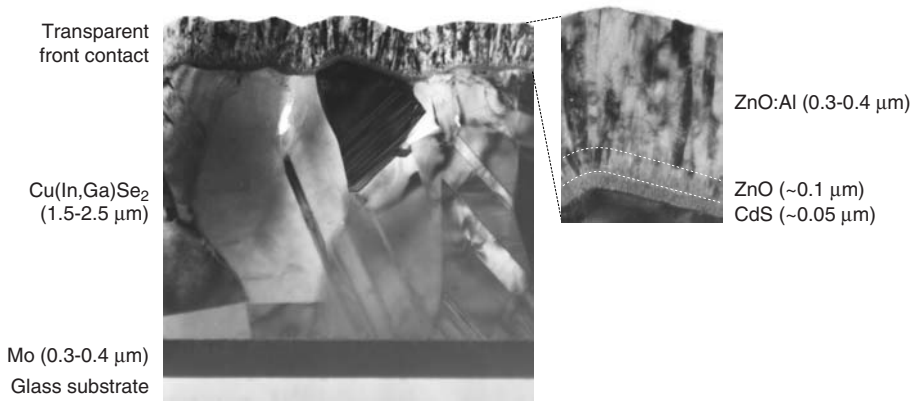

Figure 1.1: Transmission electron micrograph of a cross section of a complete CIGS device.

The substrate is soda-lime glass (SLG) with a thickness of 1-3 mm. A metal layer of molybdenum (Mo) is deposited on one side of the glass by DC sputtering. This layer is the back (+) electrode. The CIGS layer is the semiconductor where most of the solar energy is absorbed. This layer is deposited by co-evaporation from metal sources in a Se atmosphere to a thickness of 1-2 μm. During evaporation, the substrate is heated to around 500 °C. The CIGS material is doped p-type by intrinsic defects and typically has a carrier concentration of 10^{16} cm^{-3}. The doping level is not directly controlled, but

can be influenced by impurities such as Na. $CuInSe_2$ and $CuGaSe_2$ are both chalcopyrite semiconductors with direct band gaps of 1.0 eV and 1.7 eV respectively. By exchanging In and Ga in the crystal, the band gap can be varied between these values. Theoretically, a band gap of around 1.5 eV would be ideal for a solar cell. Experimentally, the highest efficiencies for CIGS have been obtained with a band gap of 1.2 eV corresponding to Ga/(Ga+In) = 0.3. More information on CIGS material properties and devices can be found in Refs. [3] and [4].

To form the pn-junction of the solar cell, an n-type semiconductor is needed. In the structure shown in figure 1.1, the junction was formed by deposition of a 50 nm thick buffer layer of CdS through chemical bath deposition (CBD). On top of the buffer layer a bilayer of ZnO is deposited by RF-sputtering. The first layer is about 50 nm of un-doped ZnO and the second about 300 nm of ZnO doped with aluminum. All top layers, CdS, ZnO and ZnO:Al, are n-type and are sometimes called the window layers, since their band gaps are so large that most of the sunlight is transmitted through the layers. The role of the buffer layers will be discussed below. The ZnO:Al layer is the front (-) electrode and is considered degenerate. To increase current collection and reduce contact resistance to the measurement probes, a thin metal grid is deposited on top of the ZnO:Al layer for the solar cells used for research. For commercial use, thin film solar cells are monolithically connected in series into modules normally without the grid, see for example Ref. [5]. This is one of the advantages of the thin film technology, however it will not be discussed in this thesis.

1.3 Device operation and efficiency measurements

The performance of a solar cell is measured by current-voltage, J(V), measurements under illumination. For accurate comparison of results, the measurements should be performed under standard test conditions. These are (i) a temperature of the device at 25°C, (ii) an illumination power density of 100 mW/cm^2 and (iii) a spectral distribution close to the AM1.5 spectrum. The latter is obtained for sunlight on earth with an incoming angle of 48.2°, i.e. the light has traversed the atmosphere 1.5 times the distance at normal incidence. In figure 1.2, dark and illuminated J(V) curves for an ideal solar cell are shown.

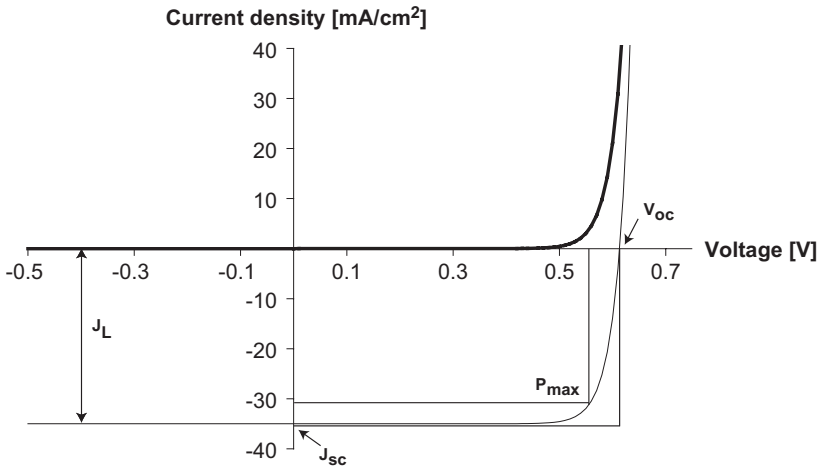

Figure 1.2: Dark and illuminated J(V) characteristics of an ideal solar cell.

In the one-diode model, the current is given by [6]

$$J(V) = J_0\left(e^{\frac{q(V-R_S J(V))}{AkT}} - 1\right) - J_L + G_{shunt}\left(V - R_s J(V)\right) \qquad (1.1)$$

where J_0 is the saturation current, A the ideality factor, J_L the light generated current, G_{shunt} the shunt conductance and R_s the series resistance. For an ideal solar cell, R_s and G_{shunt} are zero and A=1. The maximum power point, P_{max}, is the desired operating point of the solar cell. The solar cell parameters extracted from the illuminated J(V) curve are the open circuit voltage, V_{oc}, given by $J(V_{oc})=0$, the short circuit current density, J_{sc}, given by $J_{sc}(V=0)$, the fill factor, FF, given by $P_{max}/V_{oc}\cdot J_{sc}$, and the efficiency, η, given by

$$\eta = \frac{P_{\max}}{P_{in}} = \frac{1}{P_{in}} \cdot V_{oc} \cdot J_{sc} \cdot FF \qquad (1.2)$$

where P_{in} is the power in the incoming radiation.

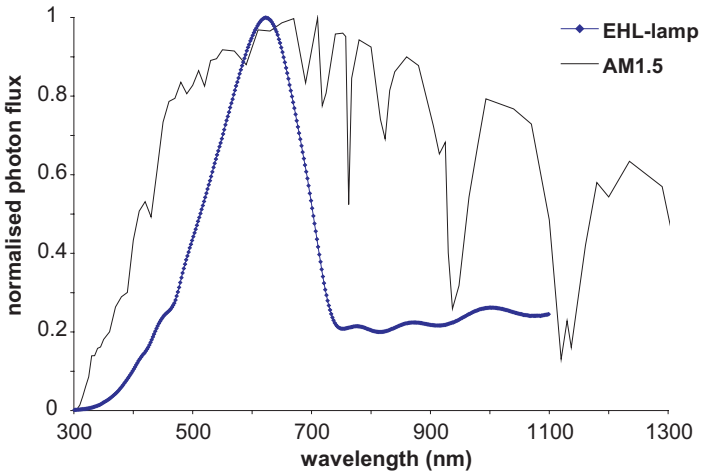

Figure 1.3: Comparison of the (normalized) photon flux from the ELH lamp used for J(V) measurements and the solar AM1.5 spectrum.

For the measurements in this thesis an ELH lamp is used for J(V) characterization, with a spectral distribution shown in figure 1.3. The temperature is controlled by a water-cooled Peltier element and the light intensity is calibrated using a reference CIGS/CdS device. Due to the difference between the spectra in figure 1.3, the J_{sc} obtained using the ELH lamp will have errors for devices with a spectral response different from the reference device. A more correct determination of J_{sc} in those cases can be obtained from Quantum Efficiency (QE(λ)) measurements. By measuring the device current as a function of photon flux in monochromatic light, the number of collected electrons as a function of number of incident photons with a certain energy is obtained. By integrating this spectral response multiplied by the AM1.5 spectra, over the total AM1.5 wavelength region, J_{sc} is obtained. This method has been used to correct J_{sc} values in this thesis, but care must be taken since devices do not necessarily show a linear dependence of J_{sc} on illumination.

1.4 The role of the buffer layer

One advantage of heterojunction solar cells (pn-junction between different semiconductors) compared to homojunctions (pn-junction with the same semiconductor on both sides) is that recombination in the wide gap semiconductor is small due to the large band gap. On the other hand, the risk for interface recombination is much larger in heterojunctions due to defects and imperfections at the interface. The role of the buffer layer, in combination with the other window layers, is to minimize interface recombination and get as large total band bending across the junction as possible. In the early days

of CIGS research, the device was made with a thick layer of CdS deposited by evaporation. A large improvement was made when most of the CdS was replaced by ZnO (as in figure 1.1), and evaporation was replaced by chemical bath deposition. The main reason for the improvement using thin CdS was reduced absorption in the window since the band gap of ZnO (3.3 eV) is larger than that of CdS (2.4 eV). Attempts to completely remove the CdS and sputter deposit ZnO directly onto CIGS have failed. Several reasons for the role of CBD-CdS have been suggested such as protection of the CIGS against sputter damage, CIGS surface etching in the CBD, Cd-indiffusion, S-passivation, good lattice match and good conduction band alignment. A number of alternative materials and deposition methods have been investigated in order to replace the CdS. Some of the results are shown in table 1.1.

Table 1.1: Efficiencies of devices with Cd-free buffer layers and the current world record CdS device. The CIGS layers are made by co-evaporation or rapid thermal processing and the composition close to the interface to the buffer layer is not equal in all cases. [a] active area, [b] with antireflective coating.

Buffer material	Deposition method	Efficiency	Reference
In_2S_3	ALD	16.4%	[7]
ZnInSe	evaporation	15.1%	[8]
In(OH,S)	CBD	15.7%[a,b]	[9]
ZnS(O,OH)	CBD	18.6%[b]	[10]
Zn(O,S,OH)	CBD	14.2% (mini-module)	[11]
Zn(O,S)	ALD	16.4%	This thesis
ZnO	ALD	13.9%	[12]
ZnS	Ilgar	14.2%	[13]
Zn(Se,OH)	CBD	13.7%[b]	[14]
(Zn,Mg)O	sputtering	12.5%	[15]
(Zn,Mg)O	ALD	14.1%	This thesis
CdS	CBD	19.5%[b]	[16]

1.5 Why avoid cadmium?

CIGS based solar cells with a CdS buffer layer have already proven high efficiency [17] and stability [4] and are commercially available. Its relevant to ask why years of research should be spent on finding a replacement. Cd is present in the soil and is taken up by the roots of plants and is found in most foods. The concentration is in general low (<0.02mg/kg) but can be higher in for example liver, kidney (up to 36 mg/kg) [18], shellfish and some mushrooms. The daily intake of Cd is about 10-20 μg, but higher for smokers. When Cd is taken up by the body, it accumulates mainly in the kidneys. With increasing Cd accumulation the function of the kidney can deteriorate. The recommended maximum weekly intake of Cd according to the WHO is

7 μg/kg bodyweight, but there are concerns that negative effects on the kidney can appear already at that exposure level. Since the main Cd intake is from basic foods, a reduction in the Cd exposure can only be obtained by reducing the background concentration in the soil.

The concentration of Cd in a CIGS/CdS module was calculated to about 0.9 weight % of the deposited material [19] excluding the substrate and cover glass. From the 1st July 2006 two new directives, *Directive on the Restriction of the Use of certain Hazardous Substances in Electrical and Electronic Equipment* (RoHS) and *Waste Electrical and Electronic Equipment Directive* (WEEE) will regulate the use of toxicants and heavy metals such as Hg, Cd, Pb in electronic products within the EU. At the time of writing, the maximum concentration value for Cd within RoHS was not decided, but the proposal [20] is 0.01% weight in "homogenous materials that cannot mechanically be disjointed into different materials". It is not clear how this would be interpreted in the case of CIGS modules. In the first 4 year time span, solar modules are excluded from RoHS and WEEE, but not solar cells implemented in consumer products since they are expected to enter the main waste stream [19].

Another concern is the exposure to Cd as well as thiourea, which is toxic and carcinogenic, during CBD-CdS fabrication. However, with the appropriate safety measures the exposure of workers can be avoided [21]. In conclusion, Cd in solar modules is not completely forbidden yet, and Cd-pollution can be avoided if recycling and take-back of modules is assured. Still, a Cd-free device is clearly a better option if device function and cost can be comparable to the CdS case.

2. Film growth by atomic layer deposition

Atomic layer deposition (ALD), or atomic layer epitaxy (ALE) as it is sometimes referred to, became widely known in the 1980's after pioneering work by T. Suntola and co-workers although parallel early ALD work was made in the Soviet Union by the group of Prof Aleskovskii [22]. The technology was initially developed by Michrochemistry Ltd in Finland, but as the advantages of the ALD technique became known, the industry has grown considerably. The main attribute of ALD is the possibility for thickness control down to the monolayer level, even on very rough surfaces and without the need for advanced external process control. Instead, the control is based on self-limiting surface reactions. The applications of ALD that currently receive the most attention are high-k gate oxides, storage capacitor dielectrics and copper diffusion barriers in advanced electronic devices.

2.1 Theory

ALD is a development of chemical vapour deposition (CVD). Both methods rely on the chemical reaction between reactants in the vapour phase (precursors) to form a thin film coating on a substrate while the reaction by-products, that should be volatile, are pumped out of the reaction chamber. In CVD the reaction can occur both at the surface of the substrate or in the gas mixture. Depending on process parameters such as temperature, pressure, gas velocity etc, the CVD reaction can be limited by 1) how much of the reactants that are introduced (thermodynamic control), 2) the diffusion of reactants to the surface and of by-products from the surface (transport control) or 3) adsorption and surface diffusion of reactants, nucleation and desorption of by-products (kinetic control). For high step coverage, kinetic control is desirable since this will give an equal deposition rate in every point of the substrate without precise control of gas velocity and precursor concentration. In ALD the elegant solution to obtaining absolute surface reaction control is to separate the reactants into sequential pulses alternated with purging of the reaction volume. The steps in an ALD process are shown schematically in figure 2.1.

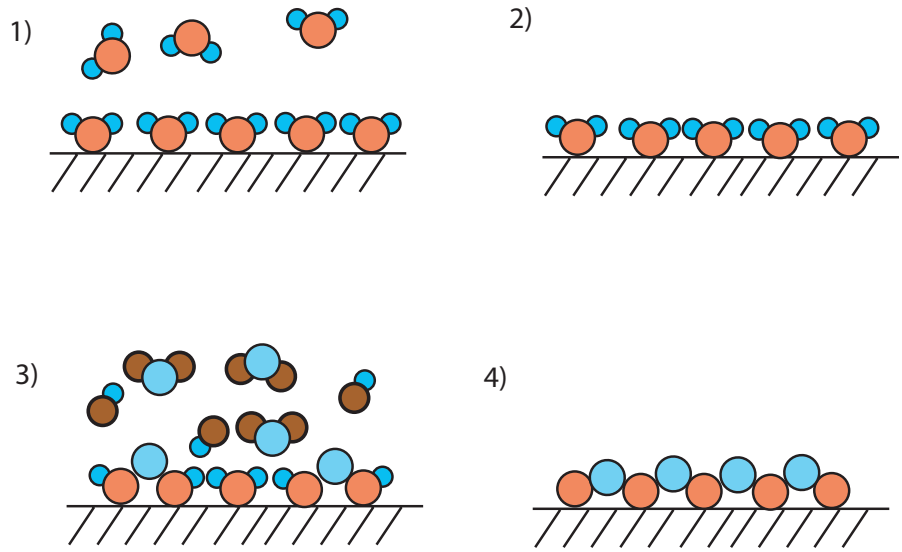

Figure 2.1. Steps in a typical ALD process, 1) chemisorption of precursor until surface saturation, 2) purging with inert gas, 3) chemisorption of second precursor and reaction until surface saturation and 4) purging.

The first precursor is introduced into the reaction chamber, adsorbs and reacts with the surface. The dose of the precursor should be adjusted to obtain surface saturation, i.e. all available surface sites should be used for reaction with the precursor. When this is obtained, the precursor inlet is closed and the reaction chamber purged with an inert gas leaving only the layer of reacted species on the surface. The second precursor is introduced and reacts with the first layer forming a monolayer of the desired material while the by-products desorb and are pumped out. This pulsing sequence corresponds to one ALD cycle. The sequence can be repeated up to the desired number of cycles and ideally the thickness is controlled on the monolayer level. As will be discussed below, monolayer per monolayer growth is an idealistic view and is not completely true for many real cases.

The density of reacted species on the surface after a precursor pulse depends on the density of available surface bonds and the size of the formed species. If a precursor consists of a molecule with large ligands, these can cover a significant fraction of the surface resulting in less than a full monolayer per cycle. The density of available surface sites can also vary significantly. In many ALD reactions OH-groups on the surface are expected to be the main bonding site. The density of surface sites can sometimes be changed with pre treatments. If several different bonding options are possible with different activation energies, the density of available surface sites can vary with temperature. Surface reconstruction and contaminants on the surface can also change the number of surface sites. In some processes it is

necessary to activate the surface, i.e. create surface sites, in between the precursor pulses.

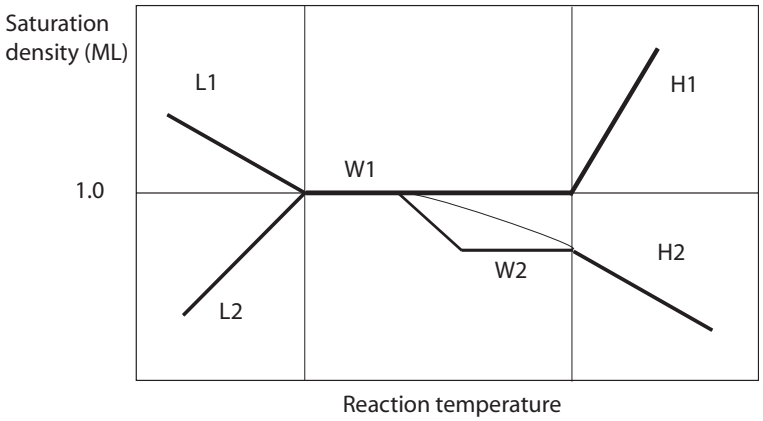

Figure 2.2. Processing window for saturated monolayers.

The processing window for ALD growth with saturated surface reactions in each pulse can be seen in figure 2.2 where the growth rate per cycle is given as a function of the reaction temperature (from Ref. [23]). Two cases can be observed on the low temperature side depending on the limiting mechanism. L1 will result if condensation of the precursor occurs at low temperature and L2 if the energy for the reaction is insufficient. Within the saturation regime a single plateau is seen if the saturation density is constant. If two or more plateaus are seen the saturation density varies with temperature as mentioned above. Disordered surfaces can have a continuously changing saturation density since a large number of bonding options with different activation energies can exist. On the high energy side decomposition (or cracking) of the precursor into non-volatile species would result in an increased deposition rate (H1). If the precursor is stable, desorption of all surface species at higher temperature will result in decreased deposition rate (H2).

Since the initial substrate is completely different from the surface of the growing film, the saturation density will also be different initially. It has been shown for ZnS [24] and other polycrystalline films grown by ALD, that the growth includes a nucleation stage during the first cycles, after which a layer-by-layer growth can proceed. The nucleation density can be substrate dependent. For a low density, the grains will grow in three dimensions for a larger number of cycles until coalescence. This can be seen as an incubation time before constant growth rate is reached. For a polycrystalline or amorphous film, a “monolayer” in ALD growth can never correspond to a layer of atoms of a specific plane in the crystal lattice. The thickness of the

monoatomic layer obtained reflects both the achievable saturation density and the average bond length for the surface species formed.

Another deviation from the ideal layer-by-layer model is the possibility that surface saturation cannot be achieved due to interaction with the grown film. This is the case of the ZnO-ZnS system and will be discussed in 2.3.

2.2 Experimental

The ALD reactor used in all experiments in this thesis is a F-120 from Michrochemistry Ltd. It is a so-called travelling wave reactor, where a carrier gas, in our case N_2, is flowing trough the reactor with a speed in the order of 10 m/s. This is advantageous for high process speed, since a multiple hitting condition can be achieved [23]. The precursors in this thesis are all external sources, connected to the reactor via separate needle valves with magnetic pulsing. Each precursor is carried to the reaction chamber in separate glass tubes and special quartz plate substrate holders ensure that no precursor mixing is possible before the substrate is reached. The reaction chamber is heated by resistive coils and the temperature can be set differently in five temperature zones between the pulsing valves and the substrate holder. The substrate size is 5 x 5 cm^2. In most experiments, the samples were loaded into a hot reactor and were subject to 30 minutes of heating before the process was started.

The precursors used are deionised H_2O, diethylzinc (DEZ), H_2S and biscyclopentadienylmagnesium (Cp_2Mg). Standard pulsing times are 200 ms and purging time 400 ms for H_2O, H_2S and DEZ. For Cp_2Mg, standard settings are given in paper VIII. For the binary alloys, DEZ/H_2O cycles were alternated with DEZ/H_2S or Cp_2Mg/H_2O cycles. The pulsing ratio in percent for the different compositions i.e. #DEZ/H_2S cycles / # DEZ/H_2O cycles or pulsing ratio MgO:ZnO has been used to name the recipes. For example, a Zn(O,S)10% process consists of 1 DEZ/H_2S cycle followed by 9 DEZ/H_2O cycles repeatedly and a (Zn,Mg)O 1:6 process consists of 1 Cp_2Mg/H_2O cycle followed by 6 DEZ/H_2O cycles repetedly.

2.3 Growth on CIGS substrates

Although part of the ALD work in this thesis is based on depositions on glass to simplify characterization, the main interest is of course the interface CIGS/ALD buffer and the bulk properties of films deposited on CIGS. The difference between a glass and CIGS substrate is the much larger surface roughness of the CIGS, a temperature limitation probably around 200-250 °C in order not to degrade the devices and an undefined surface that easily oxidizes. The roughness poses no problem for ALD growth. As seen in fig-

ure 2.3, even deep crevices in the CIGS are easily covered with a uniform film.

Figure 2.3: Transmission electron micrograph of a deep trench in a CIGS film uniformly covered by ALD-ZnO. The top layer of sputtered ZnO does not cover the trench.

The temperature limitation can be different for different CIGS and different ALD processes. Spiering *et al.* [25] showed improving performance of CIGS/ALD In_2S_3 devices with increasing temperature up to 220°C, whereas our experiments on CIGS/ZnO is that devices are shunted above about 170°C. For the alloys, the composition is deposition temperature dependent and re-optimization of the pulsing sequence would be needed for each temperature. For Zn(O,S) and (Zn,Mg)O the deposition temperature was kept at 120°C. In ALD, the process temperature can be lowered by using more reactive precursors. For the materials of interest in this thesis, ZnO, ZnS and MgO, commercial precursors exist allowing for deposition below 200°C.

The co-evaporated CIGS films are polycrystalline with a grain size in the order of a micrometer. Depending on the growth conditions, the grains can be more or less randomly oriented. Both (112) [26] and (220) preferential orientation has been reported but even for other plane orientations the surface of the crystallites will mostly be of (112) type since this is the most stable surface [27]. The composition of the surface of thin film $CuInSe_2$ has been shown by XPS to be slightly Cu-poor with a composition close to

$CuIn_3Se_5$ [28]. Similarly, the surface of thin film $CuGaSe_2$ has been observed to be Cu-poor with a $CuGa_5Se_8$ or $CuGa_3Se_5$ composition (Refs. in [27]) although the existence of a $CuGa_3Se_5$ phase is debated.

Air-exposure of the CIGS surface will change the composition. Ternary oxides with the chalcopyrite structure do not exist [27], but after several days of air-exposure In-O, Se-O and Ga-O bonds have been observed by XPS (also shown in paper I). Na diffusion from the glass substrate is known to play an important role for improving device efficiency. On air-exposed surfaces, large amounts of Na have been observed and a correlation between Na content in the film and the amount of surface oxides has been reported by Ruckh *et al.* [29]. They also reported that no Na was observed by XPS on CIGS samples kept up to 10 days under vacuum after deposition. The CIGS surfaces in this thesis have all been air-exposed prior to ALD deposition, but the time is minimised to maximum 30 minutes. A vacuum storage (10^{-7} mbar) has been used for the cases when immediate transfer from the CIGS chamber to the ALD reactor was not possible. Despite the limited air-exposure, large variations in Na-content are observed by XPS for different CIGS surfaces.

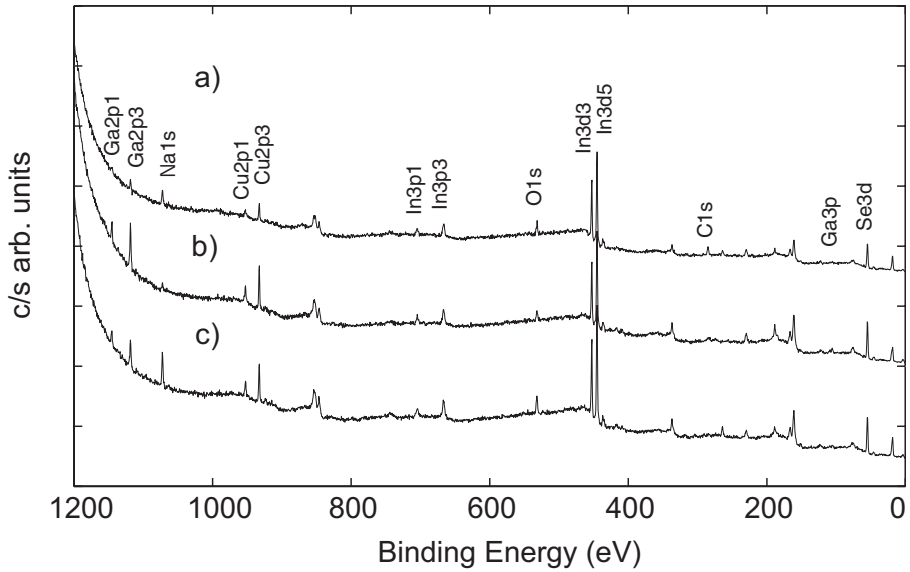

Figure 2.4. XPS overview of CIGS surfaces from three different evaporation systems. a) CIGS3, b) CIGS2 and c) CIGS1

CIGS from three evaporation systems at the Ångström Solar Center have been used, here referred to as CIGS1, CIGS2 and CIGS3. CIGS1 is evaporated in a Balzer BAK 550 system with mass-spectrometer feedback control of the metal evaporation rates [30]. Three 5 x 5 cm^2 substrates can be coated

in one CIGS1 run. The system for evaporation of CIGS2 is a modified Balzer UMS500P where the composition of the film is monitored by so-called end-point detection relying on the change of emittance that occurs when the composition of the CIGS film changes from Cu-poor to Cu-rich [31]. One 10 x 10 cm^2 substrate per run can be coated in the system. The recipe used for ALD experiments ("Cupro") is a Cu-poor - Cu-rich - Cu-poor three-stage processes as described in Ref. [31]. The third system is the micropilote line where 12.5 x 12.5 cm^2 sized substrates rotate past fixed sources [32]. In figure 2.4 an XPS overview of CIGS1, 2 and 3 surfaces, is shown. The Na content is clearly lower on the CIGS2 surface, and this has been confirmed on a number of CIGS2 surfaces from different runs with the same recipe. The Ga content is higher for the CIGS2 surface although the bulk Ga content is lower than for the CIGS1 shown in fig 2.4. CIGS3 has a strong Ga gradient due to the moving substrates and a direct comparison is not possible. However, the surface Cu content seems lower for CIGS3. CIGS1 and 2 have no intentional grading, but the surface composition could possibly be altered depending on the exact ramping down of the metal evaporation rates.

Experimentally, large variations in ALD growth have been observed for the different CIGS surfaces, especially for ZnO. Poor growth was reported by Sterner [33] on CIGS1 that had been air-exposed a few months, but a short dip in deionised water improved the growth considerably. In paper I, ZnO growth on aged and fresh CIGS1 surfaces is investigated by XPS, on surfaces with and without the water-dip, using in-vacu transfer between the ALD and XPS chamber. The water-dip was shown to wash away Na on the surface but at the same time the O1s peak shifted to lower binding energies and a C1s peak at around 290 eV disappeared. The energy could correspond to Na_2CO_3 bonding [34]. The aged, water-dipped surface showed large amounts of Se-O, Ga-O and In-O bonds, but this did not prevent ALD-ZnO growth. Therefore, the Na-C-O compound, possibly Na_2CO_3, was suggested to be the main inhibitor for ZnO nucleation. For CIGS2, the nucleation problems are less severe and ALD coatings are generally more uniform than on CIGS1. When including S in the ZnO, nucleation on CIGS is improved as seen by a smaller difference in thickness between films on glass and CIGS substrates. Another way to reduce the incubation time is to purge DEZ over the CIGS substrate for several minutes before the pulsing is started. In-vacu XPS analysis of a CIGS1 surface before and after a 5 minute DEZ pulse reveal a small decrease in O, Na and the C 1s peak at 290 eV as seen in figure 2.5. It is presently not clear how effective the DEZ surface activation is for different surfaces.

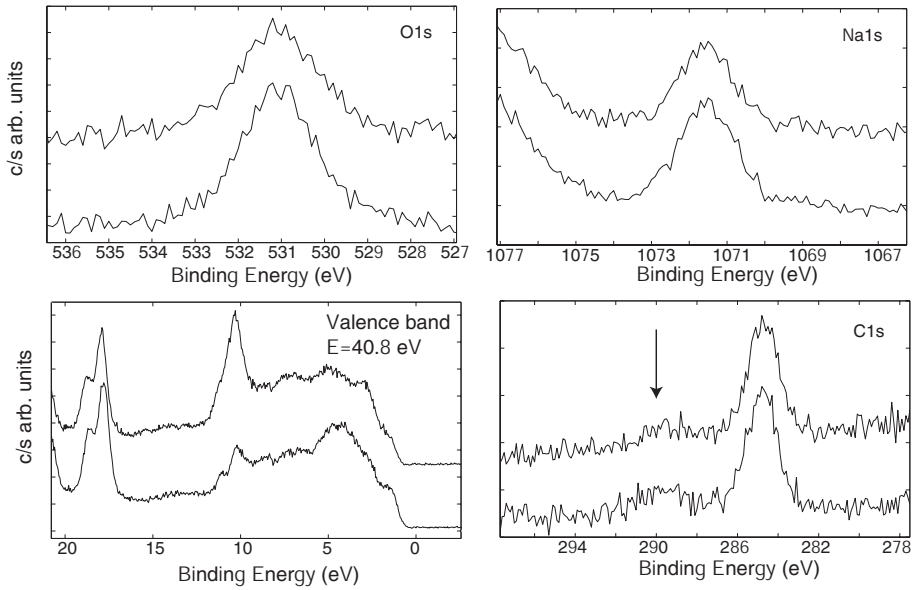

Figure 2.5. Core levels and valence band of a CIGS surface before (bottom) and after (top) a 5-minute purge of DEZ. In the valence band, the Zn3d peak at ~10eV is observed after the purge, but in the lower spectra the small peak at the same position is originating from the In 4d peak from the He II satellite line at 48.4 eV.

Another clear difference between the three CIGS types is the larger surface roughness of CIGS2 and 3. As mentioned above, a large surface roughness is not a problem for ALD growth, but could instead result in a higher nucleation density if more surface sites are present at imperfections, grain boundaries and grain edges of the rough surface. This could be another reason for the improved nucleation on CIGS2 and 3 compared to CIGS1.

Compared to the chemical bath deposition used for CdS growth, buffer deposition by ALD suffers from a clear disadvantage since no etching of the CIGS surface, comparable to that obtained in the CBD bath [35], occurs in the ALD case. The advantage of ALD on the other hand is the possibility for in-line processing of the complete solar cell structure without breaking vacuum. In such a setup, oxidation and Na accumulation on the CIGS surface would not occur and the nucleation conditions would be completely different.

2.4 Reproducibility

The reproducibility of thickness, composition and other material properties in the different ALD processes is not only dependent on the incubation time for growth, which could be substrate dependent as discussed above. Variations from run to run or over the area of the substrate could result from un-

controlled variations in substrate temperature or precursor doses. For binary compounds, thickness variations should only occur outside the ALD window for surface saturation shown in fig 2.2. The precursor doses are determined by the pulsing time, flow rate and partial pressure of the precursor. The DEZ and H_2O sources used in this thesis have no temperature control and are thus subject to fluctuations in the surrounding temperature. The H_2S source has a pressure regulator and the Cp_2Mg is temperature controlled through a heated bath. DEZ reacts violently with humid air, and deposits of powder-like ZnO will build up around leaks. The needle valves in the F-120 reactor used are sealed with rubber o-rings (EPDM) and some leaking is difficult to avoid that could cause clogging of the precursor inlet and reduced doses. For the Cp_2Mg source, condensation can occur at cold spots causing similar reduction of the inlet area. A control process, known to give a certain growth rate, can be used from time to time to check that the doses are still sufficient.

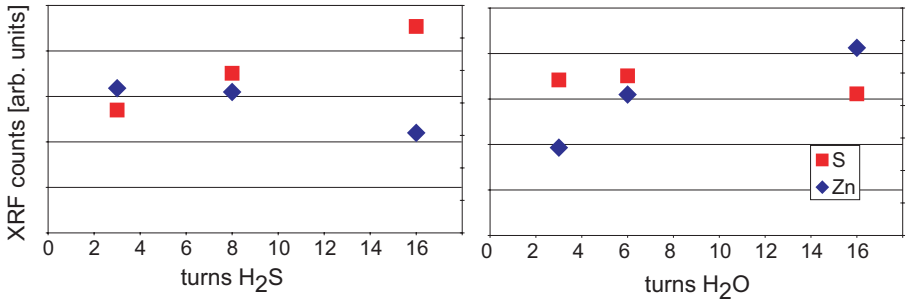

Figure 2.6. Zn and S content in Zn(O,S)8% films as a function of H_2S or H_2O dose adjusted by opening the corresponding needle valves with a certain number on turns.

For compounds like Zn(O,S) or (Zn,Mg)O the situation is more complex since activation energies could be different for growth of one compound on top of the other than for growth on the same compound. For example, in a (Zn,Mg)O process with 5 DEZ/H_2O cycles alternated with one Cp_2Mg/H_2O cycle, the surface after 5 DEZ/H_2O cycles will be very different from the surface after the following Cp_2Mg/H_2O cycle. To determine the sensitivity to process variations for the alloys, temperature- dose- and purge series should be made for each composition. This is not yet accomplished for the complete Zn(O,S) and (Zn,Mg)O series. Another complication is the possibility of exchange reactions with the grown film. This is the case for Zn(O,S) growth as discussed in paper VII. In figure 2.6 the composition of Zn(O,S)8% films are shown as a function of H_2S and H_2O dose. The composition changes continuously with changing dose and no surface saturation region can be seen. In paper VII this is discussed in terms of sulfurization of ZnO with release of H_2O or oxidation of ZnS with release of H_2S. Variations in incuba-

tion time for ZnO and ZnS growth on the different Zn(O,S) surfaces after H_2S or H_2O dosing can also affect the final composition and thickness as discussed in Ref. [36] for the ZnO-Al_2O_3 system.

2.5 Relevance for large scale production

For the ALD process to be of industrial interest, several criteria should be met. The deposition rate should be high enough so that the ALD process does not become a bottleneck in a solar module production. The growth rate for the films in this thesis is around 1-2 Å/cycle. One cycle takes 1.2 seconds giving a growth rate of 0.8 - 1.7 Å/s. For a buffer layer thickness of 30 nm the resulting deposition time is 3-6 minutes. As a comparison, the deposition time of the CIGS layer is about 15-20 minutes in this thesis. For larger areas, the ALD cycle times need to be increased to ensure complete dosing and purging, but the process speed could still be in the order of 1-4 s/cycle for batches of substrates larger than a square foot [23]. Compared to the CBD-CdS process, where the process time is only around 7 minutes, the largest gain in time for the ALD process is due to the possibility for in-line processing where removal from and reintroduction into vacuum is not needed. Currently the focus in the growing ALD industry is Si-wafer technology but there are large area applications such as thin films displays where ALD has been used successfully for over 20 years [37]. Apart from the deposition speed and availability of process equipment, the material cost must be considered. Metalorganic precursors can be expensive, 30-50 Euro/g for the ones used in this thesis, but prices vary substantially depending on the quantities bought and the required purity.

3. Film properties

3.1 Characterization techniques

A number of different characterization techniques were used in order to determine the properties of the ALD films. The film thickness on glass substrates was determined by profilometry after etching steps with dilute HCl and by x-ray reflectometry (XRR). For films deposited on CIGS, the thickness was determined from cross sections analyzed by scanning electron microscopy (SEM) and transmission electron microscopy (TEM). The intensity of the Zn signal from x-ray fluorescence was also used as a measure of thickness. Since variations in surface roughness of the CIGS layers will influence the measured signal intensity, calibration from SEM and TEM cross sections was made for samples with different CIGS deposition recipes. From TEM the microstructure and chemical properties were also determined. X-ray diffraction (XRD) was used to determine the structure, both in θ-2θ and grazing incidence mode. The film composition was determined using Rutherford backscattering (RBS), x-ray photoelectron spectroscopy (XPS) and XRF. The resistivity was determined using a four-point probe and optical properties were determined from optical spectrometry (transmission and reflectance) and ellipsometry. Some details of the characterization methods are given mainly in papers VII and VIII.

3.2 ZnO

ZnO is a group II-VI semiconductor with a number of properties such as piezoelectricity, wide band gap and n-type dopability that make it interesting for a wide span of applications [38]. ZnO can be doped n-type by for example Al, Ga and B and also shows n-type conductivity from defect doping. Zn interstitials, O vacancies and H have been proposed to be donors. Recently p-type doping by N was shown (Refs. in [38]). The band gap, 3.3 eV, can be varied by inclusion of for example Mg, Cd or S. ZnO can crystallize in wurtzite, zincblende or rocksalt structure, but only the wurtzite structure is stable at ambient conditions. The zincblende structure can be obtained on

cubic substrates and the rocksalt structure at elevated pressure [38]. Some material properties of bulk ZnO are summarized in table 3.1.

Table 3.1: Bulk properties of selected buffer materials.

	Band gap (eV)	Structure	Lattice parameter (Å)	Density [39] (g/cm^3)
ZnO	3.3 [38]	wurtzite	a=3.25, c=5.21	5.6
ZnS	3.8	wurtzite	a=3.82, c=6.26	4.1
ZnS	3.7 [40]	cubic	5.42	4.0
MgO	7.7 [38]	cubic	4.21	3.6
CdS	2.4 [41]	cubic	5.83	4.8
CdS	2.4 [40]	wurtzite	a=4.16, c=6.76	4.8

ZnO growth by ALD has been reported using $Zn(C_2H_5)_2$ [42], $Zn(C_2H_5)$ [43] and $Zn(CH_3COO)_2$ [44] zinc precursors. In most cases the oxygen precursor was H_2O but O_2 and O_3 [45] have also been investigated. The maximum growth rate is in the order of 1-3 Å/cycle for all precursors. For $Zn(C_2H_5)_2/H_2O$ which are the precursors used in this thesis, reported growth rates of 1.7-2.1 Å/cycle [46] for deposition temperatures of 140-190°C agree well with those obtained in the present work.

The ALD-ZnO films in this thesis have wurtzite structure with random orientation. The band gap, obtained from combined optical spectrometry and ellipsometry, is 3.25 eV (paper VII). ZnO has strong exciton absorption at room temperature, with a binding energy of 60 meV [38]. In paper VI, the band gap of ZnO was determined to 3.31 eV after subtraction of the 60 meV exciton energy. In the calculations of conduction band offset (CBO) however, the value 3.25 eV is used. There are two reasons for this. First, no compensation for excitons can be made for Zn(O,S) and (Zn,Mg)O since exciton energies in these materials are not known and have not been measured. When comparing the evolution of the CBO with S or Mg content in ZnO, the band gap values should be obtained with the same method for all compositions including ZnO. Second, it is not clear if the excitons are still bound in the strong field in the space charge region of the device.

The incubation time for ZnO growth was already discussed in 2.3. There are observations on an incubation time for growth even on an ALD-ZnO surface. In Ref. [46] the ALD growth from $Zn(C_2H_5)_2$ and H_2O precursors was investigated by an in-situ quartz crystal microbalance technique. An incubation time for ZnO growth was observed after interrupting the ZnO process for different times, and the incubation time increased for increasing interruption times. A complete explanation for the incubation time for ZnO growth is lacking. However, the initial growth is probably characterized by a nucleation stage followed by three-dimensional growth until coalescence.

The resistivity of ALD-ZnO is low, 10^{-2}-10^{-3} Ωcm in the present work. In Ref. [47] the resistivity of ALD-ZnO (deposited at 165°C using $Zn(C_2H_5)_2$ and H_2O) was increased from 10^{-2} Ωcm to above 10^{3} Ωcm by decreasing the flow rate of $Zn(C_2H_5)_2$. Within this thesis, some experiments were performed using an O_2 source in addition to H_2O. By adding pulses with O_2, a slightly higher resistivity was achieved. The process was not optimized for highest resistivity and it is not clear how high resistivities that can be obtained for as-deposited ALD-ZnO films. The resistivity can also be increased by post annealing in air.

3.3 ZnS and Zn(O,S)

ZnS is a II-VI semiconductor used for example in electroluminecent (EL) displays. In fact, large area atomic layer deposited ZnS:Mn for EL displays was one of the first commercial applications of the ALD technique. ZnS deposition by ALD has been reported using $Zn(C_2H_5)_2$, $Zn(C_2H_5)$ [48, 49], ZnCl [24] and $Zn(CH_3COO)_2$ [44] precursors together with H_2S. Reported growth rates are between 1-3 Å/cycle for temperatures between 100 and 500 °C. In this work, a growth rate of 1.4 Å/cycle was determined for deposition at 120 °C.

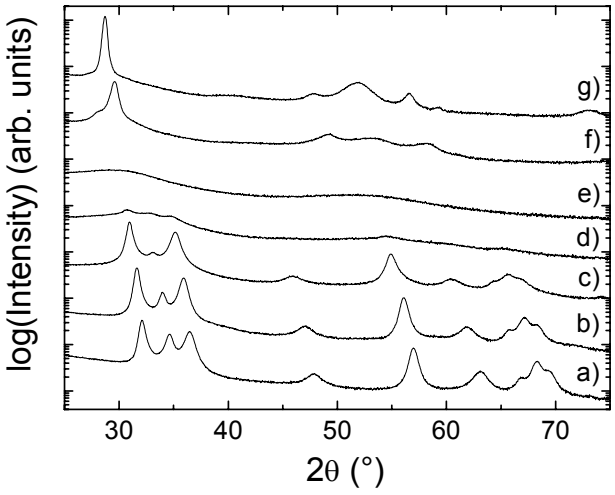

Figure 3.1: Grazing incidence diffractograms of ZnO_{1-x},S_x films: a) ZnO, b) x=0.10, c) x=0.28, d) x=0.48, e) x=0.71, f) x=0.84 and g) x=0.97.

The ALD-ZnS in this thesis exhibits a cubic or hexagonal structure with much stronger diffraction intensity from the (002) or (111) plane compared to the other planes (fig 3.1). This is not due to texture effects since diffraction with varying incoming angle of the radiation show the same intensity relation. The growth and material properties of Zn(O,S) is discussed in detail in paper VII and only the main results will be summarized here. These are (i) a larger sulfur content in the films as compared to the number of H_2S containing cycles in the process, (ii) a hexagonal ZnO structure with increasing unit cell for the O-rich side (S/Zn<0.5) followed by an amorphous or nanocrystalline region for S/Zn≈0.7 and a hexagonal (and cubic) ZnS structure for S/Zn>0.8 as shown in figure 3.1, (iii) non-linear variation of the band gap with a minimum at around 2.6 eV for S/Zn=0.5 and (iv) an occurrence of a strong sulfur gradient in Zn(O,S) films.

The determination of the band gap of the Zn(O,S) films is nontrivial and is discussed in papers VI and VII. As shown in figure 3.2 the measured absorption for ZnO and ZnS show a distinct absorption edge and direct band gap behavior. For the Zn(O,S) films however, no clear absorption edge can be defined since the absorption exhibits pronounced low energy absorption tails.

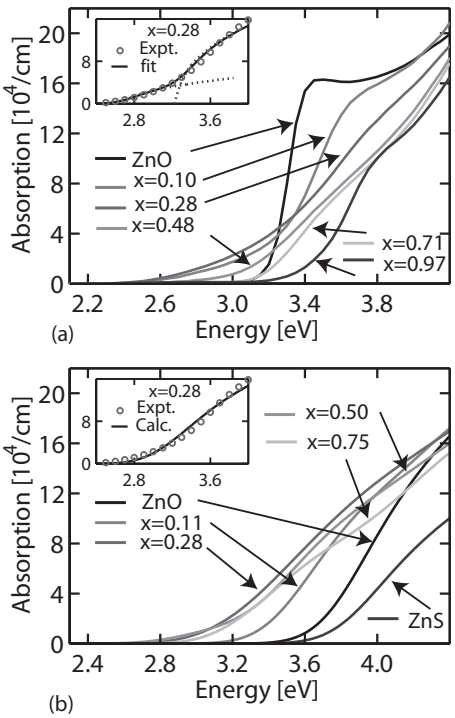

Figure 3.2 a) Measured (room temperature) and b) calculated (0 °K) absorption of Zn(O,S) films. The inset in a) shows the proposed parameterization with a sum of two direct band gaps.

In paper VI the band structure and absorption properties of Zn(O,S) was calculated from first principles and compared to the measured values of α for the ALD-Zn(O,S) films (figure 3.2). The calculations showed that local Zn-S bonds in the relatively hard Zn-O host mainly affected the valence band density of states (DOS) for O-rich films. A clear Zn-S contribution above the Zn-O dominated peak in the DOS was shown to cause a reduction of the direct band gap. Based on these results, a parameterization of the absorption according to $\alpha(E)=A(E-Eg)^{1/2}+B(E-Eg-\Delta Eg)^{1/2}$ was proposed, where Eg is the band gap of ZnO for O-rich films and that of ZnS for S-rich films. For the amorphous film, for which k-vector conservation is no longer imposed, a so-called Tauc-plot was used to extract the band gap. For the film with x=0.48 band gap extraction is difficult due to the two-phase structure of the film (figure 3.1 d). However, fitting to a combined direct band gap and Tauc expression, in order to account for both the crystalline and amorphous parts of the film, gave reasonable agreement with measured data. The obtained band gap values show a large bowing with a maximum ΔEg compared to E_g(ZnO) of 0.7 eV. This agrees well with reported band gaps of pulsed laser deposited Zn(O,S) [50] while others have reported on a much smaller bowing [51, 52]. The large variation in reported band gaps is not surprising given the different optical methods used and the non-distinct absorption edge of Zn(O,S). However, since the band structure calculations (paper VI) show that direct transitions at the Γ point indeed contribute to the low energy absorption, this tail must be included in the band gap extraction, for example by using the parameterisation shown above.

3.4 (Zn,Mg)O

The band gap of ZnO can also be varied by inclusion of Mg. Experimentally, alloying with up to 33% Mg/(Zn+Mg) has been shown [53] before MgO segregation occurs. A maximum band gap of around 3.9 eV can be obtained for the single phase wurtzite (Zn,Mg)O. There is a large interest in $Zn_{1-x}Mg_xO$ for applications such as quantum well structures and UV light emitting diodes. To our knowledge, ALD $Zn_{1-x}Mg_xO$ has not been reported prior to the work in this thesis. ALD MgO and $MgAl_2O_4$ [54] have been investigated using $MgCp_2$ and H_2O precursors. By MOCVD, $Zn_{1-x}Mg_xO$ growth using $Zn(C_2H_5)_2$, $Mg(EtCp_2)$ and H_2O precursors has been demonstrated [55].

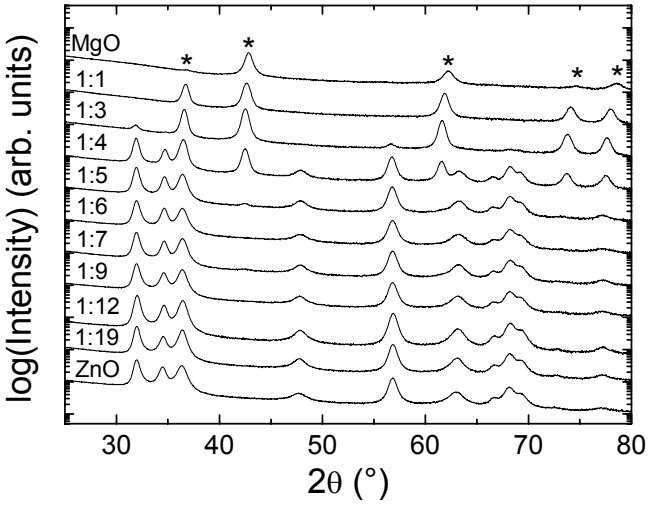

Figure 3.3: Grazing incidence diffractograms of Zn_{1-x},Mg_xO films. Films with intermediate compositions are labeled according to the pulsing sequence (MgO:ZnO). Peaks marked with an asterisk correspond to the cubic MgO phase and all unmarked reflection originates form the hexagonal ZnO structure.

In this work, Mg inclusion of up to about x=0.2 is obtained for deposition at 150 °C before MgO segregation occurs. The lower Mg content in our work compared to for example [53] could be due to differences in deposition method and temperature. However, to be able to discern a small MgO peak from XRD, good statistics are needed which is not always the case in the literature. Details of the ALD growth are given in paper VIII.

The band gap of $Zn_{1-x}Mg_xO$ as a function of Mg content in this work (fig 3.4) follows the values in the literature within the experimental errors. The determination of the Mg content from XRF is difficult due to the low intensity of the Mg-Kα signal. Other methods for compositional determination would need to be investigated in the future for higher accuracy. The band gap is determined from transmission and reflectivity measurements, using an approximate relation for obtaining the absorption coefficient (paper VIII). This method is in general less accurate than the fitting procedure used in paper VI and VII. However, no difference in band gap is obtained for ZnO using the two methods.

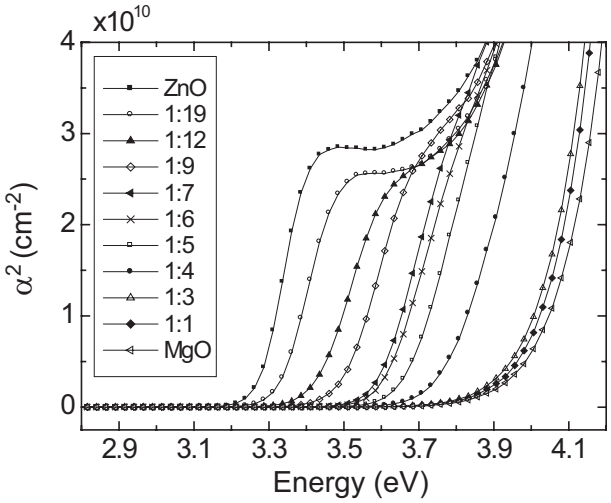

Figure 3.4: Absorption of $Zn_{1-x}Mg_xO$ films.

4. Energy band alignment at the CIGS/buffer interface

4.1 Theory

When two semiconductors with different band gaps are brought into contact a heterojunction is formed. One of the main differences of heterojunctions compared to homojunctions is the discontinuity in the valence- and/or conduction bands that must form at the interface due to the difference in band gap. The so-called Anderson model [56] deals with an ideal heterojunction with a perfect, abrupt interface free from cross diffusion, interface states and dipoles. The band diagram of such an interface is shown in figure 4.1.

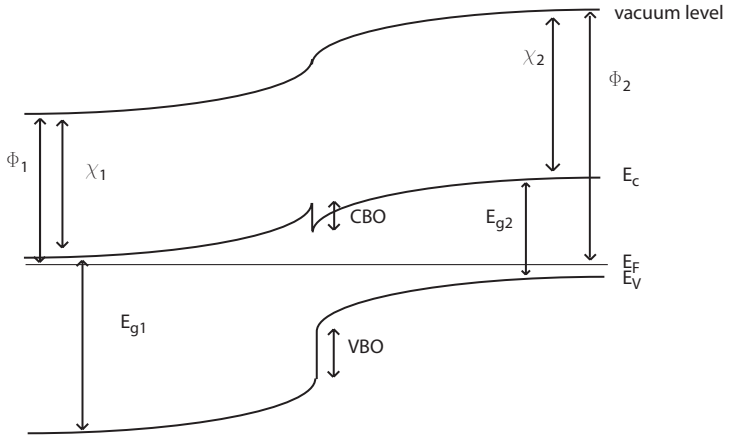

Figure 4.1: Ideal heterojunction according to the Anderson model.

The electron affinity, χ, of a crystal is the energy required to lift an electron from the bottom of the conduction band, across the surface, to a position outside the crystal called the vacuum level. Sometimes the work function, ϕ, is used instead, being the energy between the Fermi level and the vacuum level. In the Anderson model, the conduction band offset, CBO (or ΔE_c), at the interface is given by the difference in electron affinity, χ_2-χ_1, of the two materials. Similarly, as seen in figure 4.1, the valence band offset, VBO (or ΔE_v), is given by VBO= E_{g1} - E_{g2} - CBO.

For a real interface, the band alignment can be altered by interface states, dipoles, cross diffusion, strain and intermediate compound layers. In fact, the assumption of abrupt interfaces with well-defined electron affinities for a particular material fails even for stochiometric single crystals. The work function is highly dependent on the surface properties and is in general different even for in-equivalent surfaces of the same single crystal. This also means that the local vacuum level just outside one surface can be different from that outside another surface of the same crystal [57]. The interruption of the periodic lattice at a surface causes a distortion of the charge distribution at the surface compared to the bulk. To minimize their energy, electrons can spill out of the surface plane forming a surface dipole layer that increases the work function. Another possible effect is smoothing of the electronic charge, causing a dipole with the opposite orientation that lowers the work function [58]. Reconstruction of the surface will of course also change the charge distribution. Adsorption of impurity atoms on a single crystal surface has been observed to change the work function drastically in some cases. A well known example is cesium adsorbtion on tungsten whereby the work function can be lowered by up to 5 eV [59] depending on the Cs coverage.

Going back to the interface of a heterojunction, a similar situation, with dipole layers forming at the interface, is possible. In this case the "impurity atoms" could either be atoms from the other semiconductor or foreign impurities such as O, H, C etc depending on how the interface is fabricated. The effect of a dipole layer on the heterojunction in fig 4.1 can be seen in figure 4.2.a).

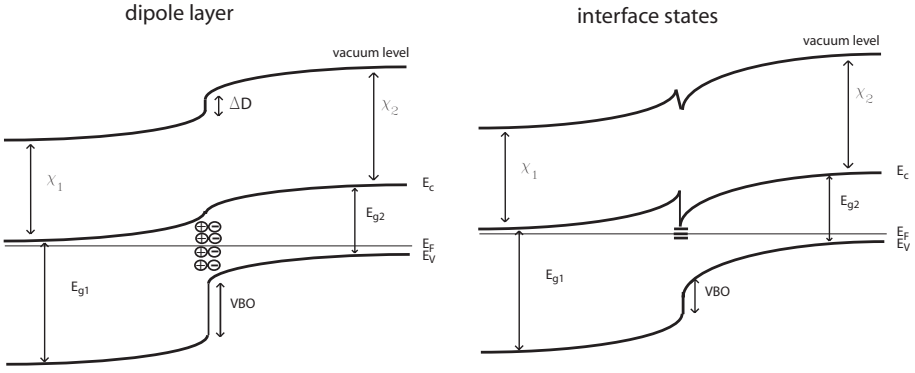

Figure 4.2: a) band diagram of a heterojunction with dipole layer at the interface where ΔD is the potential energy difference caused by the dipole and b) the same junction but with interface states. Note that an opposite orientation of the dipole would increase the CBO instead. In the right figure donor states pin the Fermi level of semiconductor 2. Acceptor states would have the opposite effect.

Another alteration of the Anderson model would arise from interface states within the band gap. These states can either be acceptors or donors and cause band bending towards the interface. For a sufficiently high density of interface states, the position of the Fermi level in the band gap can be pinned. This is well known for some metal-semiconductor interfaces, where the (Schottky) barrier height at the interface is not determined by the difference in metal work function and semiconductor electron affinity, but by surface states at the interface [40]. The effect of surface states on the heterojunction in fig 4.1 can be seen in figure 4.2.b).

In the extreme case, with a heterojunction formed by joining two semiconductor surfaces with pinned Fermi levels, the band discontinuities are completely determined by the surface states. For most real cases, the situation is probably in between that of the Anderson model and the pinned case. Interface states can also act as recombination centers and the charge states can in some cases be altered by bias and illumination.

Cross diffusion and intermediate layer formation can give rise to changes in material properties such as band gap and electron affinity resulting in an interface layer with graded band alignment. The density of localized states can be both increased and decreased due to cross diffusion.

4.2 Transport and recombination at the CIGS/buffer interface

The carrier transport across a heterojunction is greatly affected by the band discontinuities. A thorough description of the device current in a heterojunction solar cell as a function of voltage and illumination can be found in Ref. [60] and for CIGS devices in Refs. [4, 61]. Here, only some aspects relevant for understanding of the effect of the band alignment and interface defects are discussed.

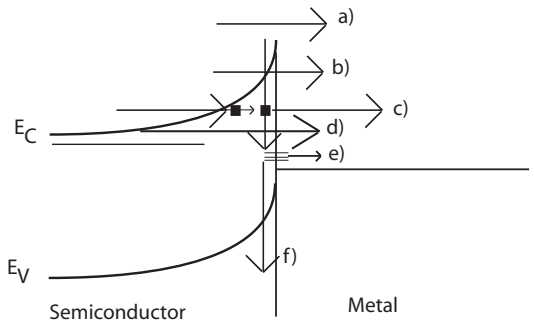

Figure 4.3: Transport mechanisms across an interface barrier, see text.

Different transport mechanisms across a barrier are illustrated in figure 4.3 for the case of a semiconductor – metal interface under forward bias (from Ref. [60]). Path a) is thermionic emission, b) thermally enhanced field emission, c) multistep tunneling, d) field emission, e) trap assisted emission and f) recombination. While the probability for thermionic emission increases with temperature, the probability for pure field emission (tunneling) increases with decreasing barrier height and width. In the case of thermally enhanced field emission, carriers are not restricted to tunneling at the bottom of the barrier, where it is widest. The carrier transport in the CIGS/buffer interface region is often modeled by assuming thermionic emission, but in some cases, it can be tunneling enhanced.

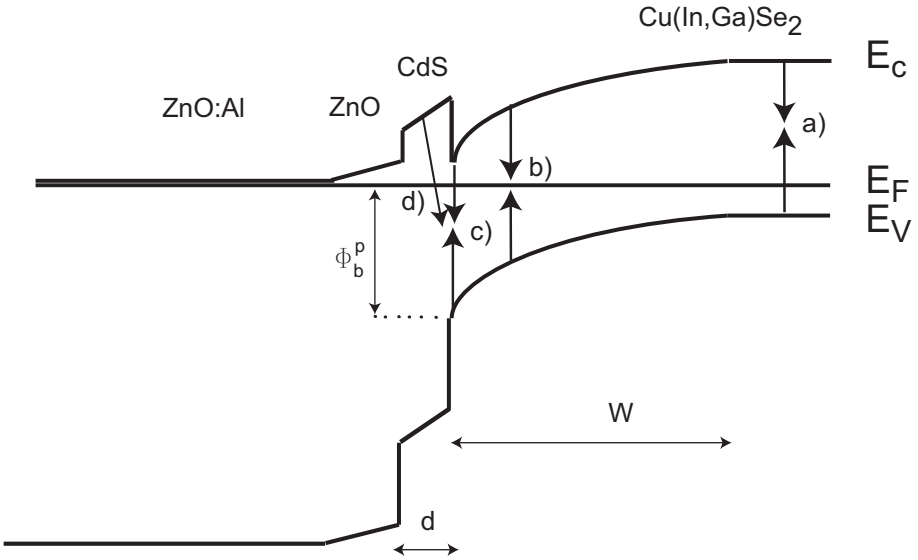

Figure 4.4: Band diagram of a CIGS/CdS device including recombination paths a-d, see text. W is the width of the space charge region in the CIGS and d the width of the buffer layer. ϕ_b^p is the hole barrier for interface recombination.

In figure 4.4 a suggested band diagram of a CIGS/CdS solar cell is shown. The photogenerated current is directed from left to right, i.e photogenerated electrons must pass the CIGS/CdS interface barrier to reach the front contact while photogenerated holes drift and diffuse to the back contact. The recombination current is directed from right to left and the different recombination paths are marked in figure 4.4. These are a) recombination in the quasi neutral region (QNR) in the absorber, b) recombination in the space charge region (SCR) of the absorber, c) interface recombination over the absorber band gap, and d) interface recombination between the buffer layer conduction band and absorber valence band. Paths b-d can be tunneling enhanced. Back contact recombination is not dominant in most CIGS solar cells. First, the absorber thickness (1.5-2 μm) is in general larger than the

carrier diffusion length (0.5-1.5 μm (Refs. in [62]). Second, the existence of an intermediate layer of $MoSe_2$, formed on the Mo surface during absorber growth, has been observed [63]. This is a material with p-type conduction and a band gap of 1.3 eV, providing a back surface field for electrons and a low resistive contact for holes. Recombination in the window layers is not significant either due to their large band gap. Note that the CIGS surface is inverted in figure 4.4, which moves the pn-junction into the absorber. This would explain why interface recombination is not dominating in high efficiency CIGS/CdS devices. The inversion could be due to the band alignment and doping at the CIGS/CdS interface or pinning of the Fermi level at the CIGS/buffer interface.

When the solar cell is illuminated, electron-hole pairs are generated mainly in the CIGS SCR. This is due to the large absorption coefficient of CIGS, but for photon energies closer to the band gap of CIGS, the absorption is weaker and this long-wavelength radiation is absorbed further into the absorber layer. Some high-energy photons can be absorbed in the buffer layer depending on its band gap. Some or all of the carriers generated in the buffer layer are not collected as seen from a reduced spectral response in the wavelength region for CdS buffer absorption. This could be due to a high recombination velocity for holes crossing the interface. The net current density can be written as [60]

$$J = J_{Generation} - J_{\mathrm{Re}combination} = e\int_{-d}^{W+L} G_L(x)dx - J_{ir} - e\int_{0}^{W+L} R(x)dx \qquad (4.1)$$

where G_L is the generation function, J_{ir} interface recombination (paths c and d) and R the CIGS recombination function (paths a and b). The integration boundaries are shown in figure 4.4, L is the width of the QNR. The open circuit voltage is the point in the J(V) curve with J = 0, i.e. $J_{Gen} = J_{Rec}$, in other words the voltage for which the barrier for recombination through paths a-e is reduced enough to cancel J_{Gen}. It should be noted that the diode characteristics are not in general independent of illumination for CIGS solar cells, as seen from the cross-over of dark and light J(V) curves.

Recombination over the band gap, assisted by trap levels, is described by Shockley-Read-Hall (SRH) formalism. This is the dominating recombination mechanism in CIGS devices [61], due to the large density of defects in the material. The recombination rate in the case of a single trap level, E_t, can be written [40]:

$$R = \frac{\sigma_p \sigma_n \upsilon_{th}(pn - n_i^2)N_t}{\sigma_n\left(n + n_i \exp\left(\frac{E_t - E_i}{kT}\right)\right) + \sigma_p\left(p + n_i \exp\left(-\frac{E_t - E_i}{kT}\right)\right)} \qquad (4.2)$$

where σ are capture cross sections for holes and electrons, υ_{th} the carrier thermal velocity, N_t the trap density, E_i the intrinsic Fermi level and n_i the intrinsic carrier density. The recombination rate reaches a maximum where n equals p and for trap levels close to midgap. For efficient CIGS/CdS devices recombination path b) is found to dominate. When the CIGS surface is inverted and n=p within the absorber SCR, the recombination will also be largest at the pn-junction according to eq. 4.2 if interface recombination is small.

For interface recombination through path c or d the current can be written [61]:

$$J_{ir}(V) = qN_v S_i e^{-\phi_b^p / kT}(e^{qV/AkT} - 1) \qquad (4.3)$$

where S_i is the interface recombination velocity and ϕ_b^p the barrier between the absorber valence band and Fermi level at the interface. In the case of a negative CBO at the interface, the distance between the conduction band of the buffer and the valence band of the absorber is lowered below that of the band gap of the absorber. This leads to a lower barrier for cross-interface recombination (path d), and is also expected to affect the inversion of the absorber surface. For negative CBO, electrons at the absorber side of the interface will lower their energy by flowing to the buffer side of the interface and thus the inversion will decrease [27, 64].

Simulations of J(V) characteristics of CIGS devices for varying CBO and interface recombination velocities, S_i, have shown a linear decrease of V_{oc} with increasing negative CBO for fixed S_i. However, for small S_i (10^3 cm^{-2}), a slightly negative CBO (-0.15 eV) can be tolerated [27]. Since holes are minority carriers at the inverted interface, they limit the recombination. If the inversion decreases, p increases at the interface causing increased interface recombination. Since in a real device, inhomogenieties in CBO can exist, an average value above 0 eV could be preferable.

For a positive CBO, the flow of electrons from the absorber can be blocked. However, simulations have shown that barriers below 0.3 eV [65] or 0.4 eV [66] do not impede the electron transport. This can be seen from the approximate equation for thermionic emission current for electrons across the CIGS/CdS interface used in one of the simulations [65]:

$$j_e \approx q v_{th} N_D e^{-|\Delta E_c|/kT}\left(e^{\Delta E_{Fn}/kT} - 1\right) \qquad (4.4)$$

where v_{th} is the carrier thermal velocity, N_D the donor density in the buffer layer, ΔE_{Fn} is the discontinuity of the electron quasi Fermi level at the buffer/ absorber interface. For $v_{th} = 10^6$ cm/s and $N_D = 10^{17}$ cm^{-3}, a CBO of up to about 0.3 eV will still give a current density in the order of 40 $mA \cdot cm^{-2}$ even for small values of ΔE_{Fn}. However, this is for the case of a n^+p type junction. For positive CBO, the current density would decrease rapidly for $N_D/N_A < 1$. J(V) curves simulated with the SCAPS software [67] with varying CBO at the CIGS/buffer and buffer/ZnO interfaces are shown in figure 4.5. The buffer layer was modeled using CdS material properties with $N_D = 10^{17} cm^{-3}$ and $N_A = 10^{16}$ cm^{-3}.

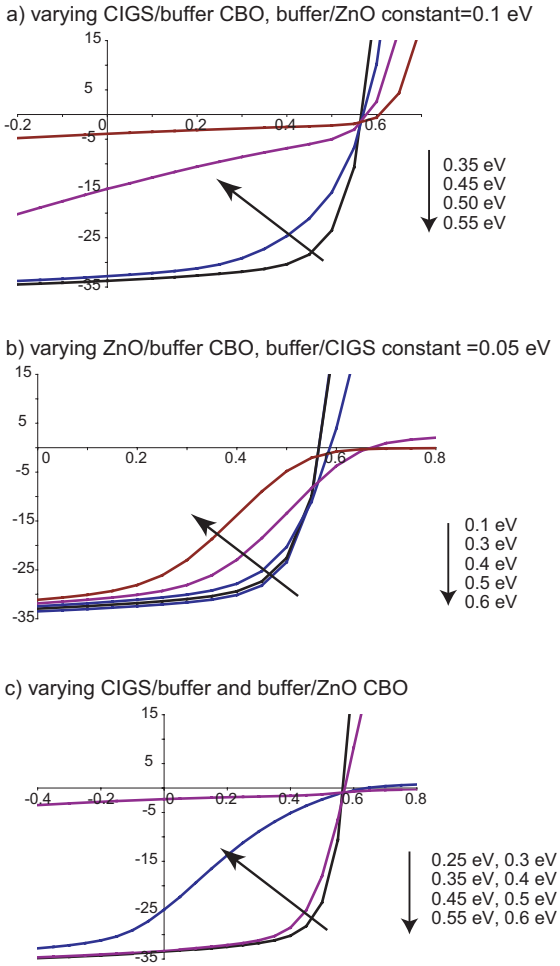

Figure 4.5: Simulated J(V) curves of CIGS/buffer devices where the CBO at a) the CIGS/buffer interface was increased and b) the buffer/ZnO interface was increased and c) both the CIGS/buffer and buffer/ZnO were increased. In this case the conduction band of the buffer was always above that of the CIGS and the conduction band of the ZnO always below that of the buffer. All CBO values are absolute values.

As seen in figure 4.5, an increased CIGS/buffer CBO is first seen as a lowered FF and for higher CBO the J_{sc} is reduced. For increasing CBO at the buffer/ZnO interface, a barrier is introduced for electrons flowing from the ZnO:Al towards the absorber in forward bias, as seen from the blocking behavior above V_{oc}. At the same time, the effective barrier for photo-generated electrons increases due to a larger distance between the Fermi-level and conduction band maxima of the buffer, caused by the increased buffer/ZnO CBO.

Since the behavior shown in figure 4.5 for large CIGS/buffer CBO has been observed from CIGS/CdS devices illuminated with red light (λ>600nm), but not with white light illumination, a light modulated interface barrier was proposed [68]. Since only photons with λ< 520 nm would be absorbed in the CdS buffer layer (Eg=2.4 eV), the effect was explained by buffer photoconductivity that would lower the barrier when the doping level in the buffer increases (increasing N_D/N_A). Another explanation for the double diode behavior, based on a p+ layer in the surface region of the absorber has been proposed [69]. The p+ layer, with a large density of localized negative charges, would form a secondary barrier in the absorber but close to the interface that could be reduced by excess holes generated in the buffer or absorber surface under white illumination. Red light illumination or reverse bias has the opposite effect. This has been explained by diffusion of positive Cu ions towards the absorber bulk leaving behind negative V_{Cu} [70] or as an electronic effect including defect relaxation [71]. The observation of cross-over in CIGS/ZnO devices, where no absorption in the buffer layer is expected, supports the model of a barrier within the absorber [72]. Of course a simultaneous barrier, light modulated or not, can exist due to a positive CBO at the buffer/absorber interface.

As shown in figure 4.5, the buffer/window interface can also influence the device. In Ref. [73], a large negative influence on the FF of CIGS/In(OH,S)/ZnO/ZnO:Al devices was found, explained by acceptor states at the CBD-In(OH_x,S_y)/sputtered-ZnO interface. The acceptor states could cause an increased buffer conduction band level relative to the Fermi level giving a similar effect as that shown in figure 4.5b for increasing CBO at the buffer/ZnO interface. The FF improved (from 20% to 70%) by including a thin CdS layer between the In(OH,S) and ZnO, and the main improvement of the CIGS/CdS/ZnO structure compared to CIGS/In(OH,S)/ZnO was concluded to be a more beneficial buffer/window interface in the CdS case.

The nature of the interface states is of great importance, not only from their ability to alter the position of the Fermi level, but also since they can act as recombination centers. From equation 4.2 it was seen that a trap level within the band gap is more effective as recombination center the closer to midgap it is situated. Consequently, shallow levels do not contribute significantly to the recombination, but can still have a large impact on the J(V) characteristics as mentioned above.

4.3 Measurement of the valence band offset by photoemission spectroscopy

In 4.2 the large influence of the CBO on device performance was discussed and in 4.1, the sensitivity of the band alignment to interface states was shown. Form this it is clear that both the establishment of a desired CBO and the measurement of its real value are important experimental challenges.

The method used for determination of valence band offset in this thesis is based on x-ray and ultraviolet photoemission spectroscopy (XPS and UPS). This is a surface sensitive technique with a probing depth of a few nm. For the XPS analysis, non-monochromatic Al Kα (1486.6 eV) and Mg Kα (1253.6 eV) radiation was used and for UPS the He I (21.2 eV) and He II (40.8 eV) lines were used. The kinetic energy of the photo-emitted electrons is given by

$$E_{Kin} = h\nu - E_B - \phi \qquad (4.5)$$

where E_B is the binding energy of the electron and ϕ the spectrometer work function. Since the attenuation length of electrons has a minima for E_{Kin} between about 10 and 100 eV [34], UPS in general and XPS of high binding energy electrons is more surface sensitive than low binding energy electrons in XPS. The spectrometer work function is calibrated from a sputter cleaned Ag sample, and adjusted so that the Ag Fermi edge from UPS is at zero binding energy and Ag core level peaks from XPS at their reference values (for example Ag $3d^{5/2}$ at 368.3 eV [34]). The spectrometer is a modified Leybold-Heraeus LHS-10 system equipped with a hemispherical electron energy analyzer and data collection is made with the SPECTRA software. Analyzer base pressure is in the low 10^{-9} mbar range.

The band alignment is measured by analyzing the valence band and core levels of (i) a CIGS surface, (ii) CIGS with thin overlayers of the buffer material and (iii) CIGS with thick buffer overlayers where only signals from the buffer layer are detected. In the case of an abrupt interface and homogenous buffer layer composition, the VBO can be obtained by comparing the distance between the valence band maxima (VBM) and a core level (CL) for the CIGS and thick buffer films separately. The relative VBM positions are then obtained from the distance between the CIGS and buffer core levels determined from spectra with thin buffer films on CIGS (eq 4.6). This indirect method [74] is needed when the valence bands of the two materials cannot be distinguished in the spectra where signals from both films are detected.

$$VBO(CIGS/buffer) = \Delta E^{CIGS}_{VBM,CL1} - \Delta E^{buffer}_{VBM,CL2} + \Delta E^{CIGS/buffer}_{CL1,CL2} \qquad (4.6)$$

As made clear in section 4.1, the band alignment of a real interface can be highly influenced by the interface formation. Therefore it is important to also measure the alignment on structures as close to the real device as possible. For CIGS/CBD-CdS interfaces, this is difficult since the chemical bath method is not compatible with UHV, and the CdS surfaces will be air-exposed prior to introduction into the analysis chamber. The starting CIGS surface will also be different from the etched surface in the ammonia containing bath. The surface contamination can be cleaned by sputtering, but this can change the surface. For some surfaces, sputtering followed by annealing in vacuum can result in well-defined surfaces [34] but this is not always the case, especially not for semiconductors. Investigations of CIGS/PVD-CdS can be made without air-exposure, but the obtained VBO cannot be transferred directly to the CBD-CdS case.

ALD is a low-vacuum technique and can be coupled to a UHV chamber through in-vacu transfer. This was made by Sterner and coworkers in our group as described in Ref. [75]. The transfer rod, originally used to introduce samples into the XPS chamber was used in the coupled XPS-ALD system to transfer samples between the XPS chamber and a modified ALD reaction chamber. The difference between the ALD reaction chambers in the coupled system and original F-120 system is a smaller substrate size, horizontal (instead of vertical) substrate position and different reaction volumes. The gas flow was vertically directed in both cases. As long as saturation is achieved in each ALD pulse, these differences should not change the growth. For Zn(O,S) however, where saturation is not achieved for H_2S and H_2O pulses (section 2.4, paper VII), the composition of the films (measured by using the Zn Auger parameter, see paper III and VII) obtained for a certain process in the coupled system was compared to the composition obtained in the F-120 system to assure that differences due to the reactor design variations had not influenced film composition.

One effect that is not taken into account in the VBO measurements is the air-anneal (2-4 minutes at 200°C) often performed on completed devices. The effect from annealing on J(V) parameters will be discussed in chapter 5, but the main effect is an improvement of V_{oc} and FF in most cases. The anneal could change the band alignment trough diffusion and redistribution of defects. However, since the trend in V_{oc} and FF as a function of buffer layer does not change after the anneal, no major change in CBO is expected.

The results from band alignment studies were reported in paper I for CIGS/ZnO, paper II for CIS/ZnO, paper III and VII for CIGS/Zn(O,S) and CIGS/ZnS. For CIGS/(Zn,Mg)O no measurement has not yet been performed, but from literature [76, 77] the VBO is expected to be close to CIGS/ZnO for Mg contents below 0.2. The results are summarized in table 4.1.

Table 4.1: Measured VBO relative to CIGS, buffer layer band gap and calculated CBO for various buffer layers. * Position according to calculations and photoemission threshold values (paper VI), ** Based on literature [76, 77]

buffer	S or Mg content	VBO (eV)	Eg (buffer) (eV)	CBO (eV)
ZnO		-2.3	3.3	-0.2
ZnO/CIS		-2.2	3.3	0.1
$ZnO_{1-x}S_x$	x=0.3	-1.8*	2.7	-0.2
$ZnO_{1-x}S_x$	x=0.7	-1.7	3.0	0.2
$ZnO_{1-x}S_x$	X=0.8-0.9	-1.3	3.1	0.7
ZnS		-1.2	3.6	1.2
$Zn_{1-x}Mg_xO$	x=0.2	-2.3**	3.6	0.2

The conduction band offset is negative (i.e buffer layer conduction band below that of the CIGS) for ZnO and $ZnO_{0.7},S_{0.3}$. For higher sulfur contents the position of the buffer layer conduction band increases giving a small positive value of the CBO for $ZnO_{0.3},S_{0.7}$ and large CBO of 1.2 eV for ZnS. For $Zn_{0.8}Mg_{0.2}O$ a small positive CBO is obtained. As will be discussed in chapter 5, these obtained CBO values are consistent with the device results with losses in open circuit voltage for negative CBO, high performance for small positive CBO and blocked photo-current for large positive CBO.

5. Characteristics of devices with ALD Zn-based buffer layers

5.1 J(V) characteristics

To compare J(V) characteristics of devices with various buffer layers to reference devices with CdS buffers is not always straight forward. The statistical variation can be large since so many process steps are involved. In many cases it is difficult to know when a cell is an "outlier" due to problems during processing that normally should not occur, or when the variation is an effect of the buffer layer. The reproducibility of device results will be discussed in 5.2. The other difficulty in making the comparison is due to the meta-stabilities observed in CIGS devices. The J(V) characteristics of devices can change under illumination, bias and heating, making the results dependent on the history of the device. This is discussed in 5.3. In this section, the performances of the best devices with different buffer layers are compared for an assumed optimized state. This could mean different annealing or illumination times for different cells. For most high efficiency devices, the optimized state is reached after a 2-4 minute anneal at 200°C and under white illumination ($\lambda > 300$ nm) for a few minutes. Since devices under working conditions are subject to white light illumination and operate at the maximum power point, the most relevant comparison would be made for the stabilized state under these conditions.

In table 5.1, the best single device results obtained for different ALD buffer layers are given. The result for the best CIGS/CdS reference cell is also given in each case. The illuminated J(V) curves were fitted to the one-diode model using a Matlab script by Malm [78] and the obtained diode parameters are given in table 5.1.

Table 5.1 Best single devices with various ALD buffer layers. The values in parenthesis were obtained after AR coating. All absorbers were CIGS except for samples 3 and 4 that were Ga-free CIS.

Sample no	Buffer	V_{oc} (mV)	J_{sc} (mA/cm^2)	FF (%)	Efficiency (%)	J_0 (A/cm^2)	A	R_S (Wcm^2)	G (mS/cm^2)
1) 107b2_4	**ZnO**	**415**	**31.1**	**61.9**	**8.0**	4.3×10^{-6}	1.77	7.6×10^{-1}	3.2
2) 107c_4	CdS	635	28.9	76.9	14.1	1.6×10^{-10}	1.30	5.0×10^{-1}	0.77
3) CIS: 124A_8	**ZnO**	**445**	**36.3**	**66.7**	**10.8**	9.3×10^{-7}	1.67	2.4×10^{-1}	3.2
4) CIS: 124B_1	CdS	476	35.0	71.3	11.9	1.8×10^{-8}	1.29	5.2×10^{-1}	2.26
5) MP1125.16cd-4	**Zn(O,S)10%**	**642**	**34.3**	**74.4**	**16.4**	1.1×10^{-8}	1.67	4.4×10^{-1}	0.31
6) MP1125.16d-2	CdS	624	33.3	75.8	15.8	2.3×10^{-9}	1.47	4.7×10^{-1}	0.42
7) 209b3_1	**Zn(O,S)20%+ZnO**	**675 (684)**	**30.3 (32.0)**	**74.5 (73.4)**	**15.2 (16.0)**	1.4×10^{-8}	1.84	3.1×10^{-1}	1.28
8) 209c3_6	CdS	647	24.7	77.1	12.3	3.3×10^{-10}	1.40	4.3×10^{-1}	1.03
9) 192A3_4	**ZnS+ZnO**	**616**	**30.1**	**65.1**	**12.1**	3.6×10^{-6}	2.68	1.8×10^{-2}	1.82
10) 192A_4	CdS	649	28.1	77.1	14.0	3.4×10^{-10}	1.39	4.0×10^{-1}	0.73
11) MP2682b-13	**(Zn,Mg)O 1:6**	**605**	**32.0**	**72.7**	**14.1**	1.2×10^{-8}	1.61	5.5×10^{-1}	1.04
12) MP2682a-18	CdS	613	29.7	75.0	13.7	7.9×10^{-10}	1.38	6.2×10^{-1}	0.95

The CIGS/ZnO device shows a 200 mV decrease in V_{oc} compared to its reference, a 2 mA/cm^2 gain in J_{sc} and a 15% unit decrease in FF. For a Ga-free absorber, the overall efficiency increases for the ZnO buffer case. Compared to its CIS/CdS reference the loss in V_{oc} is only 30 mV, in FF 5% units and the gain in J_{sc} 1 mA/cm^2. As was shown in paper II, the gain in J_{sc} was attributed both to reduced short wavelength loss (no CdS absorption) and slightly improved long wavelength collection, as seen from QE measurements. The interference was more pronounced for the ZnO devices, which is expected from the refractive index match [79]. The loss in V_{oc} was attributed mainly to the measured negative CBO of –0.2 eV for CIGS/ZnO whereas for CIS/ZnO, the measured small positive CBO (+0.1 eV) explains the improvement. In Ref. [80], the dominating recombination paths of the four device structures CIGS/ALD-ZnO or CdS and CIS/ALD-ZnO or CdS were investigated by temperature dependent J(V) measurements (JV_T). In that method, an activation energy, E_a, is determined from the relation [4]

$$J_0 = J_{00} e^{\frac{-E_a}{AkT}}$$

where J_0 is the saturation current determined by fitting of the J(V) curves to the one-diode model, J_{00} is a temperature independent constant and A the ideality factor. In Ref. [80], a modified Arrhenius plot was used to take into account the temperature dependence of A. For all structures except CIGS/ZnO, an activation energy close to the absorber band gap was obtained, indicating dominance of absorber bulk recombination. For CIGS/ZnO, E_a= 0.5 eV was obtained which is considerably lower than the band gap and indicate dominance from interface recombination. The small V_{oc} loss observed for CIS/ZnO still indicates worse interface formation than for CIS/CdS, and according to the one-diode model fit, the saturation current of the CIS/ZnO device is almost 100 times larger than for CIS/CdS. This could either be due to contribution from interface recombination enhanced by interface states at the CIS/ZnO interface or decreased inversion of the absorber. As pointed out in Ref. [61] E_a=E_g does not necessarily imply that interface recombination can be ruled out.

In Ref. [72], the large deviation from ideal diode behavior of CIGS/ALD-ZnO devices was pointed out. Almost temperature independent diode parameters, large ideality factor (>2) and high shunting currents were observed and tunneling was found to dominate the transport mechanisms. This makes fitting to the standard one-diode model questionable. However, as seen in table 5.1, the two best ZnO devices, in their optimized state, have ideality factors below 2, and reasonably good fits to the one-diode model were obtained. In Ref. [72], a weaker Fermi level pinning was also observed for the CIGS/ZnO device compared to CIGS/CdS. The reduced FF of the ZnO de-

vices compared to CdS could partly be explained within the p+ layer model discussed in chapter 4 where the internal barrier in the absorber interface region is assumed to be reduced by holes photogenerated in the buffer. For ZnO, which has a larger band gap than CdS, this positive effect would be much weaker. Another explanation for the low FF could be voltage dependence in the current collection [6] if the diffusion length in the absorber is small and the SCR width becomes too small for efficient collection at forward bias. Indeed, in Ref. [72], the total SCR of the CIGS/ZnO device was determined to around 200 nm, compared to about 400 nm for CIGS/CdS. On the other hand, slightly improved long wavelength collection was observed by QE(λ) measurements at zero bias for the ZnO devices compared to CdS (paper II). The reason for the discrepancy could be that the devices were measured in different meta-stable states.

The conclusion from the above results could be that the solution to the unfavorable band alignment and low performance of CIGS/ZnO devices would be to omit the Ga. However, CIS, with a band gap of 1 eV is not optimal for matching with the solar spectrum [2]. Instead a band gap of around 1.5 eV would be ideal. Also, for modules, a trade-off with higher voltage and lower current would be advantageous for reducing resistive losses why an increase rather than decrease of Ga would be desirable.

When including sulfur in the ZnO buffer layer, the efficiency for CIGS devices improves remarkably. The efficiency of the device with a Zn(O,S)10% buffer is the highest of all ALD-buffer devices obtained within this thesis. The J(V) and QE(λ) measurements of the two devices in table 5.1 (Zn(O,S)10% and CdS reference) are shown in figure 5.1.

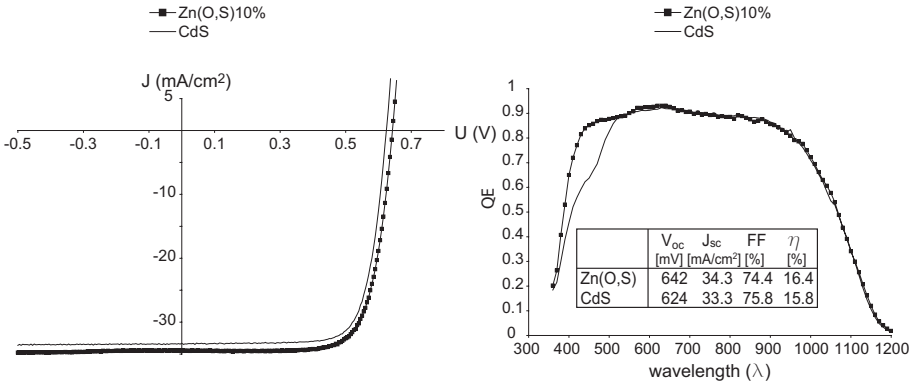

Figure 5.1: J(V) and QE(λ) characteristics of the Zn(O,S)10% device in table 5.1 and its CdS reference cell.

The Zn(O,S)10% buffer layer was 20-30 nm thick and had a S/Zn ratio of 0.3 with more S close to the interface with CIGS. The efficiency is superior to the CdS reference with a 20 mV gain in V_{oc}, 1 mA/cm^2 gain in J_{sc} and 1%

unit loss in FF. The current gain for the device in figure 5.1 is attributed to reduced buffer layer absorption in the short wavelength region only. No interference is observed from the QE measurement, and this is probably due to the rough surface of the CIGS in this case. The FF loss is small in this case. From the diode parameters (table 5.1) it can be seen that the FF loss does not appear to be caused by increased R_S or G. Possible reasons for the reduced FF could instead be a larger interface barrier than with CdS or voltage dependent current collection. The interface barrier could either be caused by a positive CBO at the CIGS/buffer interface or the p+layer within the absorber interface region. The ΔV_{oc} between the Zn(O,S)10% and CdS devices was observed to depend on Zn(O,S) buffer layer thickness. In paper V, devices with 45-50 nm thick Zn(O,S)10% buffer layers were shown to exhibit around 30 mV decrease in V_{oc} compared to their CdS references.

A comparison of CIGS/Zn(O,S)8% (with increased H_2S dose) and CIGS/CdS devices was made using CIGS deposited in two different evaporation systems as shown in figure 5.2. The J(V) parameters are given in table 5.2. The CIGS systems were described in section 2.3.

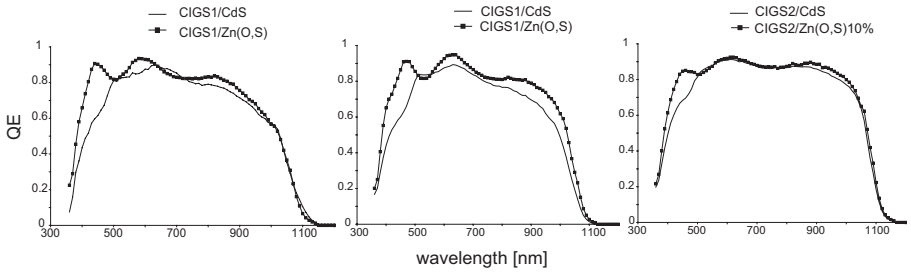

Figure 5.2: QE of Zn(O,S)8% and CdS devices. a) 250 cycles on CIGS1, b) 400 cycles on CIGS1 and c) 250 cycles on CIGS2.

Table 5.2: J(V) parameters of the devices in figure 5.2

	Est. buffer thickness (nm)	V_{oc} (mV)	J_{sc} (mA/cm^2)	FF (%)	Efficiency (%)
a) CIGS1/Zn(O,S)	15	636	31.2	71.7	14.2
CIGS1/CdS		626	29.3	76.8	14.1
b) CIGS1/Zn(O,S)	30	629	31.2	66.6	13.1
CIGS1/CdS		644	28.1	77.6	14.0
c) CIGS2/Zn(O,S)	25	525	34.0	71.6	12.8
CIGS2/CdS		605	32.7	73.7	14.6

The general observation from a large number of experiments including those shown in table 5.2 is that the ΔV_{oc} between CdS and Zn(O,S)10% (or 8% with high H_2S dose) depends both on the thickness of the Zn(O,S) layer and the CIGS material. For thin layers on CIGS1 and CIGS3 a gain in V_{oc} is observed. For thick layers on CIGS1 and CIGS3, and in all cases for CIGS2, ΔV_{oc} is negative. The absolute thickness for which V_{oc} losses occur seems different for CIGS1 and CIGS3. For CIGS1 (table 5.2) 15 nm is "thin" and 30 nm "thick", whereas for CIGS3 20-30 nm is "thin" and 45-50 nm "thick". Of course this can be expected to vary depending on the CIGS properties. Also, the ΔV_{oc} might be different if the CdS thickness was re-optimized for each CIGS. From QE (figure 5.2) the strongest interference is observed on CIGS1, which is expected since the CIGS surface roughness is much smaller compared to CIGS3 and CIGS2 [26]. Apart from the expected short wavelength gain, some improved long wavelength collection is observed in all cases. This could be due to an increased SCR width in the absorber using the Zn(O,S) buffer layers. The largest J_{sc} gain is seen for the thick CIGS1/Zn(O,S) sample, but this is counteracted by a large decrease in FF and some loss in V_{oc}. For CIGS2 a V_{oc} gain was never obtained despite a large number of experiments with varying thickness and sulfur content in the Zn(O,S) buffer layer. As was shown in figure 2.4 the surface of (air-exposed) CIGS2 differs from that of CIGS1 and CIGS3 by a higher Ga and lower Na content. Whether the V_{oc} behavior could be attributed to CIGS surface properties, CIGS doping levels, or to a different interface formation with Zn(O,S) induced by the CIGS surface, remains to be clarified. The bulk Zn(O,S) properties were not found to differ significantly for deposition on different CIGS as seen by GIXRD and XPS (paper V).

When the sulfur content in the buffer layer is further increased, the photocurrent will be blocked unless the film is ultra-thin. This means that the film either is thin enough to allow for tunneling or that it is not completely covering the CIGS surface. The CIGS/Zn(O,S)20% and CIGS/ZnS devices in table 5.1 were made with such ultra-thin layers followed by a protective ALD ZnO film (1000 cycles). For the CIGS/Zn(O,S)20% device, the gain in V_{oc} compared to its reference is large, 35 mV, and the J_{sc} of the CdS reference is unexpectedly low. From QE measurements of the two devices (without AR), a large improvement is seen in the long wavelength collection for the Zn(O,S)20% device. Due to the low J_{sc} of the CdS device, the efficiency is below the baseline standard. The reason for the poor long wavelength collection could be a reduced SCR width, possibly due to a higher than normal absorber doping concentration, N_A. The reason for the increase in V_{oc} for the Zn(O,S)20% device can partly be attributed to the large increase in the light current. In the diode parameters, the difference between the CdS and Zn(O,S)20% cells is mainly seen as an increase in both saturation current density and ideality factor for the Zn(O,S)20% device.

This is not a unique example of well performing ALD devices having low performing CdS references. Of course the reasons for the lower than normal performance of the CdS devices is not always known and could be different in different runs. However, it clearly shows that the CIGS properties and device structure needs to be re-optimized when exchanging the CdS with an alternative buffer layer.

For the CIGS/ZnS device, a loss in V_{oc} of 20 mV is accompanied by a large loss in FF (10% units). This could possibly be explained by the large CBO of 1.2 eV at the interface. However, since the ZnS layer is ultra-thin, the barrier height could be lower due to inter-diffusion or, in the case of non-complete coverage, negative over a small fraction of the interface. A thin barrier at the interface will cause a narrow zone with very high electric field that would increase tunneling. Both ZnS and Zn(O,S)20% devices show a drastic decrease in performance for a small increase in buffer layer thickness. This is due to blocking of the photocurrent by the barrier caused by the large positive CBO (paper VII).

The most recent results in this thesis are based on the CIGS/(Zn,Mg)O structure. The J(V) characteristics of devices with varying Mg content in the (Zn,Mg)O layer are shown in figure 5.3. J(V) parameters are given in table 5.3. In all cases the buffer layers were deposited at 120°C with 1000 cycles.

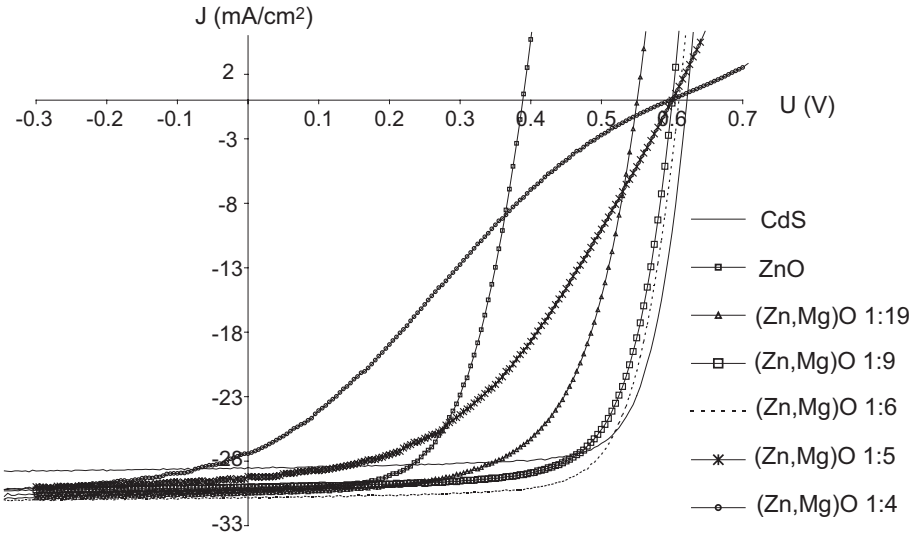

Figure 5.3: J(V) characteristics of devices with (Zn,Mg)O buffer layers. For the (Zn,Mg)O films the pulsing ratio MgO:ZnO is given.

Table 5.3: J(V) parameters of devices with (Zn,Mg)O buffer layers deposited with 1000 cycles. The pulsing ratio is given as 1 MgO: number of ZnO cycles.

Buffer layer	Voc (mV)	Jsc (mA/cm^2)	FF (%)	Efficiency (%)
CdS	621	28.5	75.8	13.4
ZnO	389	30.2	60.4	7.1
(Zn,Mg)O 1:19	551	30.5	63.0	10.6
(Zn,Mg)O 1:9	600	30.1	71.5	12.9
(Zn,Mg)O 1:6	610	30.8	73.1	13.7
(Zn,Mg)O 1:5	600	29.2	44.1	7.7
(Zn,Mg)O 1:4	597	27.4	24.2	4.0

The efficiency increases with increasing Mg content up to the 1:6 process. The increase is seen both in V_{oc} and FF whereas the J_{sc} gain is constant at around 2 mA/cm^2 for all ZnO to 1:6 processes. For even higher Mg contents, the FF decreases indicating a barrier at the interface. For the 1:6 devices (table 5.1 and 5.3), a loss in V_{oc} of 10-30 mV, a gain in J_{sc} of 2 mA/cm^2 and a loss in FF of 2-4 % units result in efficiencies close to, and in some cases above, the CdS references. For the devices shown in table 5.3 the V_{oc} is always lower for the (Zn,Mg)O devices compared to the CdS references. This is also the case for the CIGS3/(Zn,Mg)O device shown in table 5.1. This could be due to higher interface recombination for the (Zn,Mg)O devices. Since sulfur has been reported to passivate interface trap states, the inclusion of a thin S-containing layer at the interface could be beneficial.

Contrary to the Zn(O,S) case, (Zn,Mg)O devices where not improved by thinning of the buffer layer. Instead a decrease in both V_{oc} and FF was observed for devices with 500-cycle compared to 1000-cycle (Zn,Mg)O buffer layers.

5.2 Reproducibility of device performance

While the results in table 5.1 show a proof of concept for the Zn(O,S) and (Zn,Mg)O buffer layers, the reproducibility of the device results is crucial for implementation in an industrial production. In this section the reproducibility of the device results is discussed as the reproducibility of the ALD process itself was covered in 2.4.

High reproducibility can either be achieved by good control of all process steps making variations small, or by choosing materials and processes that show large tolerance to variations. The latter is of course preferable. For the buffer layer, three regions can play a role for the device: the CIGS/buffer

interface, the buffer layer bulk and the buffer/window interface. For the CIGS/CBD-CdS interface, one inherent advantage of the method is the etching of surface oxides, making the devices less sensitive to uncontrolled CIGS surface oxidation. For ALD, etching processes could be possible, but the real advantage of using a vacuum technique is the possibility for in-vacuum transfer. In general, if inversion of the CIGS surface is achieved through pinning by interface states (interface formation) rather than by the band alignment and doping (presumably bulk properties), a larger sensitivity to process variations could be expected.

The bulk properties of the ALD buffer layers could be different for deposition on different CIGS surfaces due to the incubation time discussed in section 2.4. Control of the incubation time could possibly be achieved through in-vacuum transfer or by including a short CVD step prior to ALD cycling. The tolerance to potential sputter damage during ZnO deposition is important both for the buffer layer bulk and the buffer/window interface. The effect from damage on the bulk film could be worse for thinner layers if a larger part of the buffer layer is affected negatively.

In real devices it is difficult to separate between the three effects. However, a clear proof of the overall larger tolerance of the CdS buffer compared to Zn(O,S)10% is seen in figure 5.4.

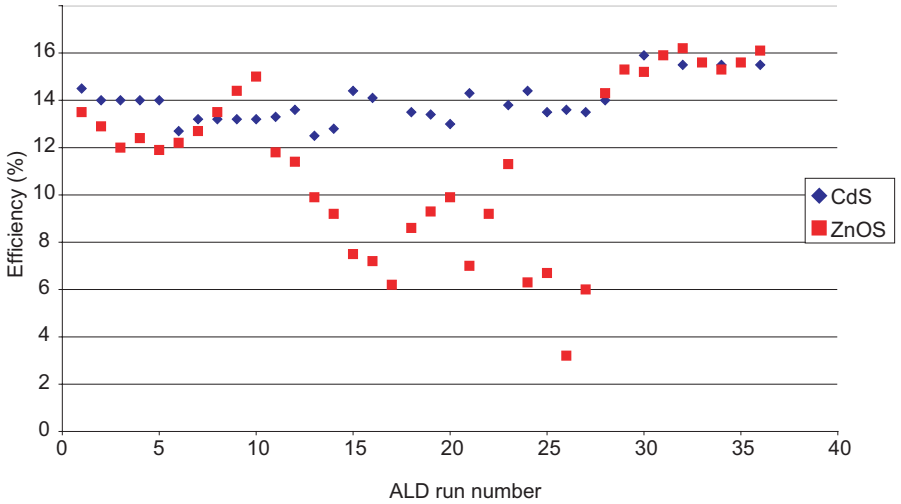

Figure 5.4: Efficiency of Zn(O,S)10% devices compared to CdS. In runs 1-27, problems with the ZnO sputtering and/or CIGS evaporation had occurred.

Problems with both the CIGS evaporation (wrong temperature in the final evaporation stage) and ZnO sputtering (leak) lead to a small decrease in efficiency for the CdS devices but a large decrease for most Zn(O,S)10% devices. The exact reason for the efficiency loss was not clear, but whatever the reason was, it affected the CdS devices much less. Without the CIGS and

ZnO problems (run 28-36), the efficiency of the Zn(O,S)10% devices improved and high reproducibility was shown in 9 consecutive ALD runs.

For Zn(O,S)20%, the main problem for high reproducibility is the varying incubation time since the layer thickness has to be controlled within a few nm. In paper IV, a process with increased pulsing times together with reduced number of cycles was used to reduce the incubation time resulting in improved reproducibility but at a lower efficiency level. The effect of the protective ZnO layer on the tolerance to variations in the sputtered ZnO or CIGS processes is not clear.

For ALD-ZnO devices, the reproducibility is very poor, which might not be surprising given the negative CBO and weak Fermi level pinning, making the recombination very sensitive to defects in the interface region. There are indications ([47] and unpublished experiments) that CIGS/ZnO devices improve with increasing resistivity of the ZnO. The reproducibility of the resistivity in the ALD ZnO process is lower than the reproducibility of thickness and that could also contribute to the variations in the CIGS/ZnO device results. For (Zn,Mg)O no investigations on the reproducibility have been made.

5.3 Stability and light-soaking effects

CIGS devices, especially those with alternative buffer layers, show a number of meta-stable effects. In the literature, these have been grouped into three types [81, 82]: 1) increased V_{oc} due to persistent photoconductivity in the absorber under red illumination ($\lambda > 680$ nm), 2) decreased FF under reverse bias and 3) increased FF under blue illumination ($\lambda < 480$ nm). The meta-stable states can relax in the dark with varying relaxation times depending on temperature. Additionally, annealing in air at around 200°C is often performed to optimize devices. For CdS devices the positive effect of annealing seems to be long-term stable, whereas this is not the case for ALD ZnO devices as will be shown below. The long-term stability of devices has not been tested systematically within this thesis, but the results of the measurements made are given below. Due to the limited statistics in these measurements and non-systematic approach, the results might not reflect a typical behavior of the device structure (if there is one). As mentioned earlier, long term outdoor testing of encapsulated devices would be the most relevant test from an application point of view. However, studies of meta-stable effects under non-realistic lab-conditions are motivated to increase the understanding of the device behavior.

The devices showing the largest instabilities are CIGS/ZnO. In figure 5.5, the V_{oc} and FF of some ZnO devices as a function of annealing time is shown.

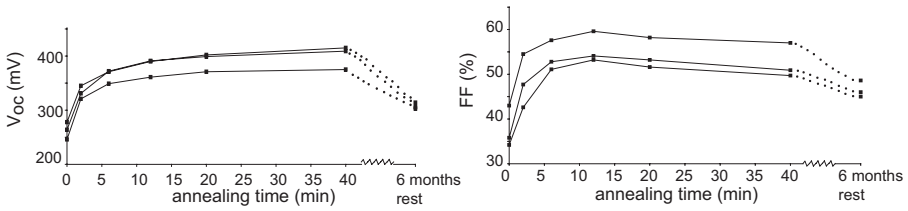

Figure 5.5: Effect of annealing at 200°C on the V_{oc} and FF of ZnO devices.

The V_{oc} of the ZnO devices in figure 5.5 improve gradually with annealing and the FF improves drastically at first and then decreases slightly. The spread between different ZnO devices in the same run is much larger than for CdS devices. After 6 months of rest in a dark N_2-flooded cabinet, the efficiency of the CdS devices is normally unchanged, while the ZnO devices in Fig. 5.5 have degraded down to a level slightly above the as-deposited state. Light soaking under white light at RT had almost no influence on the tested ZnO devices. An explanation to the effect of annealing on CdS devices was proposed in Ref. [83] as oxygenation-induced passivation of donor defects, possibly related to Se deficiency, at grain boundaries that would reduce the band bending at the grain boundaries resulting in decreased SCR recombination. Another effect of the annealing in Ref. [83] was an increased junction SCR width in the absorber and this was explained by Cu^+ diffusion to the absorber bulk causing a decrease in the effective bulk doping. In the case of ZnO, a more stable improvement from annealing is accompanied by a reversible effect. One possibility would be that the irreversible improvement for ZnO devices is due to a grain boundary passivation and the reversible effect to changes in the junction from diffusion of for example Cu. From dark J(V) characterization, the main improvement from annealing appears to be the reversible removal of severe shunts.

Zn(O,S) devices have not shown the meta-stable annealing effect seen for ZnO devices. In most cases, the effect of annealing was very similar for Zn(O,S) and CdS devices, i.e. a slight improvement of V_{oc} and FF. The exception is some Zn(O,S) devices that showed a double-diode behavior before annealing that disappeared after 2-4 minutes of annealing. The Zn(O,S) devices improve with white light and optimum values are obtained within a few minutes of light-soaking. For CdS devices, the improvement is normally faster. Some Zn(O,S)20% devices were found to degrade after storage in the dark for more than two months. The degradation mainly affected the FF, but it was found (paper IV) that light soaking at elevated temperature (100°C) for up to 60 minutes could improve the performance up to, or above, the level before degradation. No effect was seen after light soaking in room temperature or heating alone.

For Zn(O,S)10% devices, accelerated life-time tests of un-encapsulated devices in a damp-heat (DH) climate chamber (85 °C, 85% humidity) [84] showed a larger degradation for CIGS1/Zn(O,S) than CIGS1/CdS, but smaller degradation for CIGS2/Zn(O,S) compared to CIGS2/CdS. The decrease in efficiency was mainly due to FF loss for the Zn(O,S) devices. The Zn(O,S) devices appeared to be dominated by interface recombination in the dark state after DH while bulk recombination was found to dominate in the illuminated state.

(Zn,Mg)O devices have shown very large cross-over between dark (never illuminated, i.e. relaxed state) and light J(V) curves as seen in figure 5.6.

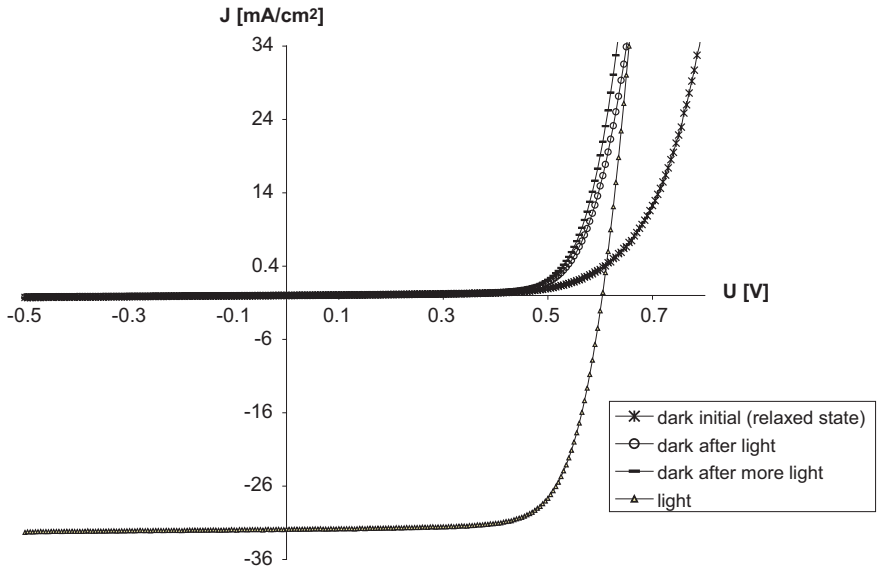

Figure 5.6: Dark and light J(V) characteristics of a (Zn,Mg)O 1:6 device.

The cross-over was most pronounced for (Zn,Mg)O 1:6. For the tested devices, the optimum state was achieved within a few minutes of light soaking and the behavior was reversible and reproducible. The long-term stability of (Zn,Mg)O devices has not been tested.

6. Additional issues regarding the CIGS/buffer interface

As already mentioned, the conduction band offset is not the only important parameter for the CIGS/buffer interface formation. Several other factors have been suggested to play an important role for the success of the CIGS/CdS interface. These will be discussed below and related to interfaces using alternative buffer layers.

6.1 Ordered Vacancy Compound (OVC) and inversion of the absorber interface region

The surface of CIGS films used for devices has been shown by XPS to have a lower Cu content than the bulk. The free surface of CIS films has been shown to have a composition close to $CuIn_3Se_5$ (In/(In+Cu)=0.75) for bulk In/(In+Cu) ratios down to about 0.52 which is close to the stochiometric $CuInSe_2$ composition [28]. In the literature the Cu-poor surface layer has been labeled ordered vacancy or ordered defect compound (OVC or ODC) and its role for the device has been widely discussed. CIS films made with a bulk composition of 1:3:5 had a band gap of 1.2 eV and were n-type conductive [85]. Since the E_F-E_{VBM} distance of non air-exposed CIS surfaces with device quality was above 1 eV (the band gap of CIS), this lead to a model of the heterojunction between p-$CuInSe_2$ and an interface layer of n-OVC [28]. No proof of the occurrence of a segregated 1:3:5 phase on the surface of absorbers used for devices has been shown by XRD, TEM or electron diffraction and this lead to the conclusion that a surface layer would have a thickness of below 15 nm [70]. The doping density of the bulk 1:3:5 films of 10^{11} – 10^{12} cm^{-3} [85] in a 15 nm layer is too low to counterbalance a typical absorber doping density of 10^{16} cm^{-3} and a SCR width of 300 nm [70]. On the other hand, surface states with a density of 10^{12} cm^{-2} could provide the charge necessary to obtain the observed inversion of the surface. The observed Cu-depletion of the surface could then be a consequence of the inversion rather than the cause of it, due to Cu migration driven by the built in electrical field [70]. The surface states responsible for the observed inversion could possibly be positive Se vacancies (V_{Se}) that pin the Fermi level close to the conduction band [86]. The inversion, seen on as-deposited CIGS lay-

ers by UPS, decreases upon air-exposure [83], and this has been explained by the passivation of V_{Se} by oxygen. According to that model, one important role of the chemical bath for CdS deposition would be the activation of the donor states through removal of surface oxides. For CIGS/CdS devices the inversion at the interface has been observed by combined admittance spectroscopy and deep level transient spectroscopy [87] from a E_F-E_{CBM} distance of about 0.1 eV. By scanning Kelvin probe microscopy, a buried homojunction located 30-80 nm from the CIGS/CdS interface was found [88].

For the case of the CIGS/ALD Zn(O,S) interfaces in this thesis, where the buffer layer is deposited on air exposed CIGS surfaces, no strong inversion due to ALD pulsing was observed by in-vacu UPS during interface build-up. All investigated CIGS films, with maximum 30 minutes air-exposure, had a VBM position 0.6-0.8 eV below the Fermi-level. After the initial Zn(O,S) pulsing, a band-bending of about 0-0.2 eV was observed resulting in E_{VBM}-E_F distances of below 0.8 eV in all cases. For a CIGS band gap of 1.2 eV this corresponds to a Fermi level position 0.4 eV below the conduction band. In the case of surface band gap widening the value becomes even larger. From JV(T) measurements of the corresponding devices and from their high V_{oc} and efficiency, interface recombination is not expected to be dominating. Whether the inversion observed after deposition of a thin Zn(O,S) film is enough to minimize interface recombination, or if further decrease of the E_F-E_{CBM} distance occurs after deposition of the complete buffer layer and window, remains to be investigated.

6.2 Cd or Zn doping of the CIGS surface

One important role of the junction formation with CBD-CdS was suggested to be n-type doping of the CIGS surface by Cd [89]. This would form a homojunction in the CIGS and interface recombination would be reduced since p=n is moved away from the metallurgical interface. Devices treated with a Cd partial electrolyte (PE) followed by ZnO deposition show a large improvement in performance compared to CIGS/ZnO devices without the Cd treatment (figure 6.1). SIMS and XPS depth profiles of $CuInSe_2$ single crystals with and without the Cd PE treatment showed a clear indiffusion of Cd in the PE case [90]. By TEM EDX, Cd in-diffusion into CIGS thin films was shown up to 10 nm from the interface with CBD-CdS deposited at 80°C [91]. TEM EDX analysis of a CIGS/CBD-ZnS interface revealed in-diffusion of Zn of about 40 nm into the CIGS after annealing at 200°C [92].

In Ref. [93] an n-type surface CIGS layer was formed by evaporation of Zn at the end of the CIGS co-evaporation process. Zn-doping in the CIGS was confirmed from SIMS profiles. By junction electron-beam induced current (JEBIC) measurements, the position of the pn-junction was found to depend on the Zn partial pressure during evaporation. For a high pressure,

the junction was found about 500 nm from the CIGS/ZnO interface. The corresponding device had an efficiency of only 2%. For lower Zn partial pressure the junction was close to the interface and the efficiency 11%. It was concluded that a thick n-type layer degrades the cell performance since the lifetime of photogenerated holes in the n-type layer will be short. This was supported by the reduced short wavelength spectral response of the highly Zn-doped devices. In Ref. [64] it is pointed out that for a given amount of charge in a type-inverted surface region, the cell performance would be maximized by minimizing the layer thickness. The minimum thickness would correspond to charge located at the interface itself, and consequently deliberate doping far into the CIGS absorber is not desirable. However, as shown by the PE experiments, Cd or Zn doping at or within 10-20 nm of the interface seems compatible with high device performance.

In paper II, Zn diffusion at CIS/ZnO and CIGS/ZnO interfaces was investigated by TEM EDX. Slight Zn in-diffusion of up to 50 nm was observed into CIS after a 40 minute anneal at 200°C, but not into CIGS. By XPS analysis of the samples after etching away the ZnO layer in dilute HCl, increased Zn intensity and decreased Cu intensity was observed on the annealed CIS sample. Since the device improvement with annealing was reversible, the observed (irreversible) Zn-diffusion after annealing was not hypothesized to play an important role for the higher efficiency of CIS/ZnO compared to CIGS/ZnO. The simultaneous increase in Zn (or Cd) and decrease of Cu has been observed by many authors and lead to the suggestion that Cd or Zn can occupy V_{Cu} in the Cu-poor surface layer [89].

The J(V) parameters and QE characteristics of a CIGS/ALD-ZnO device compared to a Cd PE-treated CIGS/ALD-ZnO are shown in figure 6.1.

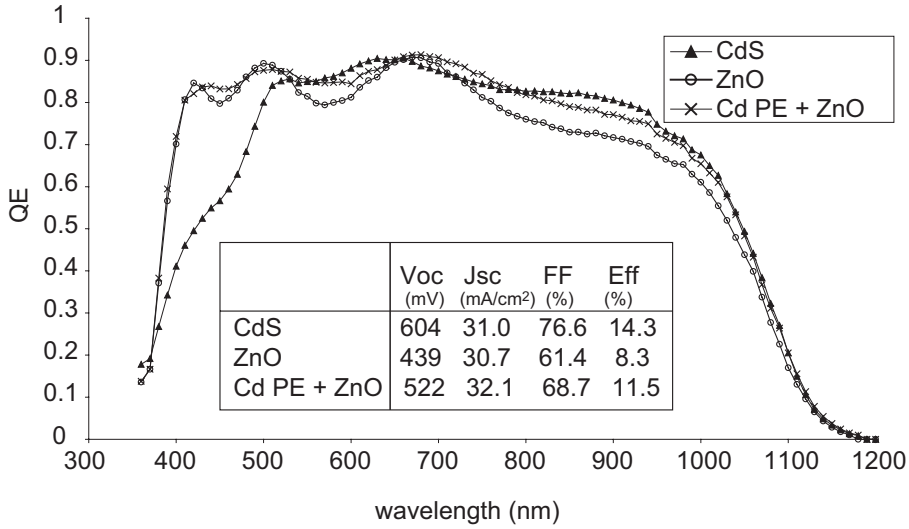

	Voc (mV)	Jsc (mA/cm2)	FF (%)	Eff (%)
CdS	604	31.0	76.6	14.3
ZnO	439	30.7	61.4	8.3
Cd PE + ZnO	522	32.1	68.7	11.5

Figure 6.1: QE characteristics and J(V) parameters of devices with CdS, ZnO and Cd PE + ZnO buffer layers.

All J(V) parameters improve with the PE treatment. From QE, reduced interference for the Cd-CIGS/ZnO sample is observed compared to CIGS/ZnO. Since the Cd-dip is not expected to increase the surface roughness of the CIGS, a possible explanation could be layer formation that changes the refractive index match. Such a layer could be composed of for example $Cd(OH)_2$ [94]. The improved performance could be due to the establishment of interface charge that pin the Fermi level and increase the inversion. Another possibility is that the band alignment with ZnO is changed. This has been reported for a $CuIn(S,Se)_2$/ZnO interface investigated by UPS and inverse photoemission spectroscopy (IPES) with and without Cd-treatment of the absorber [95]. The Cd-treatment lead to a change from a negative to positive CBO, mainly due to a lowering of the absorber band gap (lower conduction band) through the removal of a surface contamination layer.

6.3 Sulfurization of the CIGS surface

To minimize interface recombination, the hole barrier ϕ_b^p (ch 4.2) should be large. This could be achieved by lowering the CIGS valence band at the interface. By exchanging Se with S in CIGS, the valence band is lowered by about 0.2 eV and the conduction band increased by 0.2 eV [96, 97]. Another suggested beneficial effect of S at the CIGS surface is passivation of deep traps as observed from admittance spectroscopy [98].

There are a number of experimental evidences for the improvement of device performance from sulfurization of the CIGS surface. For absorbers

prepared by rapid thermal processing (RTP), the anneal in H_2Se is normally followed by an anneal in H_2S resulting in a graded surface layer with increasing S but almost no Ga at the interface [99, 100]. In Ref. [101] it was reported that small amounts of sulfur improved both V_{oc} and FF of RTP prepared CIGS, but if the sulfur content was too large, the FF deteriorated.

Post annealing of co-evaporated CIGS absorbers in an H_2S-Ar mixture at 550°C was investigated by Nakada *et al*. [102]. All J(V) parameters improved after a 3-hour anneal and S incorporation was confirmed by XRD and Auger Electron spectroscopy (AES). Wet sulfurization processes have also been shown to improve device performance [103]. Sulfurization of co-evaporated CIGS by prolonged pulsing of H_2S in an ALD reactor and by rapid thermal processing with H_2S were investigated by Sterner *et al.* [104]. The device performance degraded for all sulfur treatments and this was partly explained by the observed phase segregation between a S-containing surface layer and a Se-containing back layer. For Ga-free absorbers, no phase separation was observed and a $CuIn(S_x,Se_{1-x})_2$ layer with gradual increase of x towards the surface was observed [105]. The device performance of CIS/CdS cells improved after RTP sulfurization [106].

The high efficiency of the Zn(O,S) devices shown in this thesis could partly be due to positive effects of sulfur at the interface. From TEM EDX, no S diffusion into the absorber has been observed (paper VII) and therefore no band gap widening is expected. The high V_{oc} of the Zn(O,S) devices could instead indicate passivation of deep traps by sulfur. For (Zn,Mg)O devices, where the CBO is positive, the loss in V_{oc} compared to CdS could be due to increased trap density close to the interface. In that case, a sulfur treatment of the absorber surface prior to (Zn,Mg)O deposition should be beneficial.

6.4 Lattice matching at the interface for reduction of defect states

For heterojunctions in general, lattice mismatch at the interface should be avoided since strain and dangling bonds can form recombination centers. For CIGS/CBD-CdS, local epitaxy of {111} cubic CdS on {112} CIGS has been reported [91]. For increasing Ga content in CIGS, the lattice mismatch of the {112} plane to the {111} cubic or {002} hexagonal CdS planes increases [3]. By including Zn in CdS, the lattice match with CIGS can be improved [107]. For $CuGaSe_2$, an improved interface quality and device performance was obtained by increasing the CdS bath temperature from 60°C to 80°C [108]. For the higher temperature, intermixing at the interface was observed resulting in a non-abrupt transition from $CuGaSe_2$ to CdS. For CIGS/ALD-In_2S_3 interfaces, good lattice match was observed for In_2S_3 films deposited at

210°C [109]. This deposition temperature also resulted in the best device performance.

In paper VII, the interface between CIGS and Zn(O,S) was investigated by HR-TEM. Orientation relationships were observed between atomic layers of CIGS1 and Zn(O,S)5% and 10%. However for the investigated CIGS3/Zn(O,S)10% sample, with a device efficiency of 15.8%, this was not observed. Studies of the interface of highly efficient CIGS/CBD-ZnS devices also revealed poor lattice match [92]. These results indicate that lattice match is not an absolute requirement for obtaining high efficiency CIGS/Zn(O,S) devices.

7. Conclusions

The overall conclusion of this thesis is that the standard CdS buffer layer in $Cu(In,Ga)Se_2$-based solar cells can be replaced by Zn(O,S) or (Zn,Mg)O grown by ALD. The main explanation for high device efficiencies using these buffer layers is the optimized conduction band alignment to CIGS obtained by introducing appropriate amounts of S or Mg into the ZnO.

The band offsets at the CIGS/buffer interfaces were determined for ZnO, ZnS, Zn(O,S) and estimated for (Zn,Mg)O buffer layers. At the CIGS/ZnO interface the conduction band of the ZnO is below that of the CIGS causing increased interface recombination and consequently reduced open circuit voltage. Devices with ZnO buffer layers also show poor reproducibility and large electrical meta-stabilities. When including S into the ZnO, for S/Zn ratios up to 0.5, the valence band increases while the conduction band remains fixed. For higher S/Zn ratios the conduction band increases while the valence band remains fixed. This leads to a large band gap bowing for Zn(O,S) and implies that a S/Zn ratio above 0.5 is needed to obtain an improved CBO for CIGS/Zn(O,S) as compared to CIGS/ZnO. For compositions close to ZnS, the conduction band is too high relative to CIGS, causing a barrier for the photo-generated electrons. Two different recipes with intermediate sulfur concentrations were developed yielding high efficiency devices: ultra-thin films with S/Zn of 0.8-0.9 and around 30 nm thick films with an average S/Zn ratio of 0.3, but with increasing S content towards the CIGS surface. For (Zn,Mg)O, high efficiency devices were obtained with Mg/Zn+Mg contents of around 0.2 for which the increased band gap relative to ZnO leads to a favourable small positive CBO with CIGS.

For industrial production, both long-term stability and reproducibility of device performance are required. The stability has not been thoroughly investigated in this thesis but preliminary results indicate that devices with Zn(O,S) buffer layers show comparable stability to CdS containing devices. The performance reproducibility of devices with Zn(O,S) fabricated in this work is in general less good than for devices with CdS. This could partly be explained by the fact that new, non-optimised processes have been used but also indicates that CdS by chemical bath deposition possess a large tolerance to variations in the CIGS material and front contact which does not appear to be the case for Zn(O,S) by ALD. Further work is needed in order to optimise all materials and processes for these new buffer layers and to determine the important parameters for high reproducibility.

Summary in Swedish

Zinkoxidbaserade tunna filmer som ersättning av kadmiumsulfid i CIGS-solceller

Solceller konverterar solenergi direkt till elektrisk energi. De flesta solceller som finns på marknaden idag är gjorda av halvledarmaterialet kisel (Si). Dessa solceller har lång hållbarhet och relativt hög verkningsgrad, ca 15%, vilket är tillräckligt för kommersiella tillämpningar. Barriären för storskalig användning av solceller beror istället på det höga priset. Prisreducering är den huvudsakliga drivkraften bakom utvecklingen av så kallade tunnfilms-solceller. Den här avhandlingen ingår i utvecklingen av tunnfilmssolceller baserade på halvledarmaterialet $Cu(In,Ga)Se_2$, kallat CIGS. Strukturen hos en CIGS-solcell i genomskärning visas i figur 1.

Figur 1: CIGS-baserad tunnfilmssolcell i genomskärning.

Solcellens viktigaste funktioner är absorption av solljuset och separering av de laddningar, elektron-hål par, som skapas. En solcell är en diod, eller pn-övergång, där ett inbyggt elektriskt fält skapas mellan en halvledare med överskott på elektroner (n-dopat material) och en annan med överskott på hål (p-dopat material). Det är tack vare det inbyggda fältet som de genererade elektron-hål paren kan separeras. I CIGS-solcellen är CIGS materialet p-typ medan toppskikten, CdS och ZnO, är n-typ (Fig 1). CdS skiktet kallas buffert och målet med denna avhandling är att finna ersättningsmaterial till CdS för att undvika användningen av tungmetallen kadmium i solcellen.

De tunna filmerna i CIGS-solcellen, med en sammanlagd tjocklek på bara ca 3 mikrometer, tillverkas med olika vakuummetoder som sputtring och förångning. Undantaget är CdS-skiktet som tillverkas med en våtkemisk metod. För förenklad tillverkning av solcellerna är det önskvärt att de olika vakuumstegen kan kopplas samman utan att bryta vakuum. Därför användes en vakuummetod, atomic layer deposition (ALD), för tillverkning av de alternativa materialen i denna avhandling. I ALD förs reaktanter i gasfas växelvis in till substratet och reagerar med ytan. Eftersom reaktanterna är separerade sker reaktionen bara på substratytan. Idealt styrs ALD-processer av ytmättade reaktioner viket gör att mängden av reaktanterna inte måste styras med hög noggrannhet. ALD är lämpligt att använda för buffertskikten eftersom jämn stegtäckning erhålls redan för mycket tunna filmer även på ojämna ytor såsom CIGS. Därmed liknar ALD delvis den våtkemiska metoden.

Den enklaste lösningen för att bli av med kadmium vore att utesluta CdS ur strukturen och belägga ZnO direkt på CIGS-skiktet (jämför standardstrukturen i figur 1). Tyvärr ger detta ineffektiva solceller med låg spänning och instabilt beteende. Detta förklaras till stor del av positionen hos energibanden (valens- och ledningsbanden) vid gränsytan CIGS/ZnO. För att få låga förluster bör ledningsbandet hos buffertskiktet ligga på samma nivå eller strax över ledningsbandet hos CIGS-skiktet. För CIGS/ZnO är detta inte fallet utan ZnO-nivån ligger istället strax under CIGS. Genom att lösa in svavel (S) eller magnesium (Mg) i ZnO ändras materialegenskaperna och positionen för energibanden.

I denna avhandling visas att verkningsgraden för solceller med de alternativa materialen Zn(O,S) och (Zn,Mg)O tillverkade med ALD kan vara lika hög eller högre än för referensceller med CdS. Detta gäller Zn(O,S)-filmer med en S/Zn kvot runt 0.3 och extremt tunna Zn(O,S) skikt med S/Zn runt 0.8-0.9. För (Zn,Mg)O erhålls effektiva solceller för en Mg/(Zn+Mg) kvot runt 0.2. Dessa resultat förklaras till stor del av den gynnsamma energibandsmatchningen vid gränsytan CIGS/buffert som uppmätts med elektronspektroskopi och optiska metoder.

För industriell produktion av solceller krävs robusta tillverkningsprocesser och långtidsstabila solceller. Långtidsstabiliteten för de alternativa solcellerna är inte fullständigt testade i denna avhandling. Preliminära undersökningar visar dock att solceller med Zn(O,S) buffert är jämförbara i stabilitet med solceller med CdS-buffert. Reproducerbarheten av prestanda hos Zn(O,S)-solceller har generellt varit lägre än för CdS-celler i detta arbete. Det beror delvis på att nya processer använts men visar också på en hög tolerans hos CdS för variationer i CIGS-materialet och framkontakten som inte verkar återfinnas hos Zn(O,S). En viktig skillnad mellan ALD och den våtkemiska metoden för CdS tillverkning är att rengöring av CIGS-ytan sker i badet men ej i ALD-processen. Ytterligare arbete krävs för att optimera material och processer för en ny buffert och för att utreda vilka kriterier som är avgörande för hög reproducerbarhet.

I figur 2 visas resultatet av kvanteffektivitets- och ström-spännings-mätningar av en solcell med Zn(O,S) buffert och motsvarande referenscell med CdS-buffert. Kvanteffektivitetsmätningar (QE) visar andelen elektroner i den yttre kretsen (”användbara elektroner”) som funktion av ljusets våglängd. I figur 2b ser man att den enda skillnaden mellan CdS och Zn(O,S)-cellerna är en högre QE för Zn(O,S) vid korta våglängder. Detta beror på att Zn(O,S) har ett högre bandgap än CdS vilket resulterar i högre ström för Zn(O,S)-cellen. I figur 2a framgår att Zn(O,S)-cellen har både högre ström och spänning och att den maximala effekt som går att få ut är större för Zn(O,S)-cellen än för CdS-cellen.

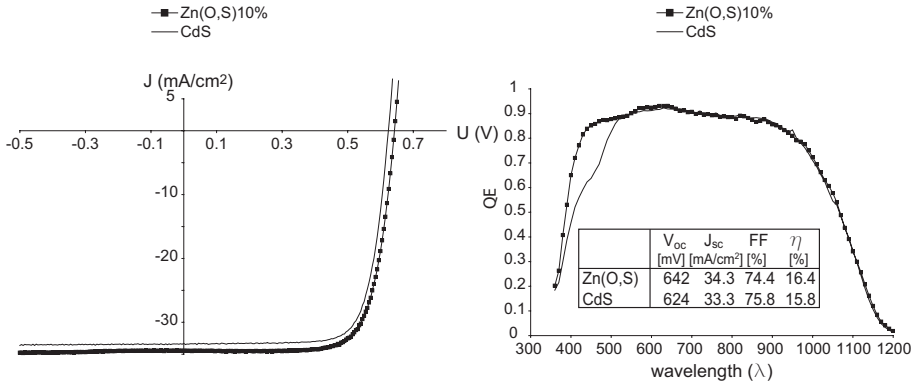

Figur 2: a) Ström-spänningskarakteristik för en solcell med Zn(O,S) buffert jämfört med motsvarande referenscell med CdS-buffert. b) Kvanteffektivitetsmätning av samma celler.

Acknowledgements

I would like to thank Lars Stolt for accepting me as a PhD student and for showing confidence in my capabilities from the start. I've appreciated your comments and ideas and your ability to identify the critical questions in my work. I also want to thank John Kessler. Your willingness to discuss and share ideas at any time, as well as your lab-skills, have meant a lot to me and this thesis. I've really appreciated that you remained long-distant supervisor after moving to Nantes. Apart from my supervisors I want to thank a number of people: Jan Sterner for giving me a thorough introduction to the XPS system and "the coffin" (ALD). Tobias Törndahl. Your ALD and XRD skills have already meant a lot for the buffer work and me. I've appreciated working and discussing with you during the last year and look forward to the continuation. Clas Persson for inspiring discussions and a great understanding of my thesis deadline stress. I hope we find more common projects in the future! Jonas Malmström for endless enthusiasm, critical proof reading and good discussions. Marika Edoff and Lars for facilitating long-distance and part time work for example by providing me with a portable computer. Marta Ruth, Marika Edoff, Olle Lundberg and Sebastian Scleussner for providing excellent CIGS absorbers. Jens Schöldström for helping me with the UMS. Torvald Andersson, Björn Kuzavas and Einar Söderman for helping me keeping the XPS and ALD leak tight and running. All nice people at the department and above all Marianne Asplund for keeping the order in a very pleasant way and Ventsi Yanchev for our discussions about science, life and Bulgaria. Lina Malmberg for doing the literature search on Cd issues, and for performing high quality experiments during and after your master thesis work. The EU-NEBULES group for pleasant and inspiring meetings. Ulf Malm for writing a user-friendly one-diode-model fitting program and for proof reading the thesis manuscript. Uwe Zimmermann for proof reading the thesis manuscript and for fixing everything in the lab with a smile. Current and previous members of the solar cell group for creating a pleasant working environment. Solar cell colleges around the world from whom I've learnt a lot and also had a good time with; Neghar Naghavi, Lothar Weinhardt, Clemens Heske and Margret Igalson to mention a few.

Smålands Nation and the Anna-Maria Lundin foundation for funding my participation at the Osaka and Barcelona conferences, and of course Glasblåsarna, maybe the best student orchestra in the world…

My supportive parents and family, Platzer and Björkman, for believing in me and also for all the valuable help with Anna.

Above all Petter and Anna for your warmth and love. Without you Petter, I would have struggled much more to keep the balance in life. You've cheered me up, pushed me forward, listened patiently to my work-related monologues and even proofread part of this thesis.

The Swedish Energy Agency, MISTRA and the European Commission through the NEBULES project for financial support.

References

1. A. Luque and S. Hegedus, eds. *Handbook of photovoltaic science and engineering*. 2003, Wiley: Chichester.

2. M. Green, *Solar Cells: Operating principles, Technology and System Applications*. 1992, Rosebery: The University of New South Wales.

3. W. Shafarman and L. Stolt, *Cu(In,Ga)Se2 solar cells*, in *Hansbook of photovoltaic science and engineering*, A. Luque and S. Hegedus, Editors. 2003, Wiley: Chichester.

4. U. Rau and H.W. Schock, *Cu(In,Ga)Se2 solar cells*, in *Clean energy from photovoltaics*, M. Arcker and D. Hill, Editors. 2001, Imperial Colleage Press.

5. J. Wennerberg, *Design and stability of Cu(In,Ga)Se2-based solar cell modules*, PhD Thesis, *Faculty of Science and Technology*. 2002, Uppsala University: Uppsala.

6. W. Shafarman, R. Klenk, and B. McCandless, *Device and material characterization of Cu(In,Ga)Se2 solar cells with increasing band gap*, Journal of Applied Physics, 1996. **79**(9): p. 7324-7328.

7. N. Naghavi, S. Spiering, M. Powalla, B. Canava, and D. Lincot, *HIgh-efficiency copper indium gallium diselenide (CIGS) solar cells with indium sulfide buffer layer deposited by atomic layer chemical vapor deposition (ALCVD)*, Progress in Photovoltaics: Research and application, 2003. **11**: p. 437-443.

8. Y. Ohtake, T. Okamoto, A. Yamada, M. Konagai, and K. Saito, *Improved performance of Cu(In,Ga)Se2 thin-film solar cells using evaporated Cd-free buffer layer*, Solar Energy Materials and Solar Cells, 1997. **49**: p. 269-275.

9. D. Hariskos, M. Ruckh, U. Ruhle, T. Walter, H.W. Schock, J. Hedström, and L. Stolt, *A novel cadmium free buffer layer for*

Cu(In,Ga)Se2 based solar cells, Solar Energy Materials and Solar Cells, 1996. **41/42**: p. 345-353.

10. M.A. Contreras, T. Nakada, M. Hongo, A.O. Pudov, and J.R. Sites, *ZnO/Zn(O,OH)/Cu(In,Ga)Se2/Mo solar cell with 18.6% efficiency*. in *Proc. of the 3rd world conference on photovoltaic energy conversion*. 2003. Osaka, Japan, p. 570-573

11. K. Kushiya, M. Tachiyuki, T. Kase, I. Sugiyama, Y. Nagoya, D. Okumura, M. Sato, O. Yamase, and H. Takeshita, *Fabrication of graded band-gap Cu(In,Ga)Se2 thin film mini-modules with a Zn(O,S,OH)x buffer layer*, Solar Energy Materials and Solar Cells, 1997. **49**: p. 277-283.

12. S. Chaisitsak, A. Yamada, and M. Konagai, *Comprehensive study of light-soaking effect in ZnO/Cu(In,Ga)Se2 solar cells with Zn-based buffer layers*. in *Proc. of the Materials Research Society Symposium*. 2001. San Fransisco, p. H9.10.1-5

13. H. Muffler, M. Bär, C. Fisher, R. Gay, F. Karg, and M. Lux-Steiner, *Ilgar technology, VIII: Sulfidic buffer layers for Cu(In,Ga)(Se,S)2 solar cells prepared by ion layer gas reaction (Ilgar)*. in *Proc. of the 29th IEEE Photovoltaics Specialists Conference*. 2000, p. 610-613

14. A. Ennaoui, U. Blieske, and M.C. Lux-Steiner, *13.7%-efficient Zn(Se,OH)x/Cu(In,Ga)(S,Se)2 thin film solar cell*, Prog Photovolt Res Appl, 1998. **6**: p. 447-451.

15. T. Glatzel, H. Steigert, R. Klenk, and M. Lux-Steiner, *Zn1-xMgxO as a window layer in completely Cd-free Cu(In,Ga)(S,Se)2 based thin film solar cells*. *Technical Digest from the 14th International Photovoltaic Scince and Engineering Conference*. 2004. Thailand

16. M. Green, K. Emery, D. King, S. Igari, and W. Warta, *Solar cell efficiency tables (version 25)*, Progress in Photovoltaics: Research and application, 2005. **13**: p. 49-54.

17. K. Ramanathan, M.A. Contreras, C. Perkins, S. Asher, F.S. Hasoon, J. Keane, D. Young, M. Romero, W. Metzger, R. Noufi, J. Ward, and A. Duda, *Properties of 19.2% efficiency ZnO/CdS/CuInGaSe2 thin-film solar cells*, Progress in Photovoltaics: Research and application, 2003. **11**: p. 225-230.

18. www.slv.se.

19. M.J.d. Wild-Scholten, K. Wambach, E.A. Alsema, and A. Jäger-Waldau, *Implications of european environmental legislation for*

photovoltaic systems. To appear in *Proc. of the 20th European Photovoltaic Solar Energy Conference*. 2005. Barcelona

20. European Commission, KOM(2004) 606, 2004

21. V. Fthenakis and P. Moskowitz, Progress in Photovoltaics: Research and application, 1995. **3**: p. 295-306.

22. R. Puurunen, *Surface chemistry of atomic layer deposition: A case study for the trimethylaluminum/water process*, Journal of Applied Physics, 2005. **97**: p. 121301.

23. T. Suntola, *Surface chemistry of materials deposition at atomic layer level*, Appl Surf Sci, 1996. **100/101**: p. 391-398.

24. J. Ihanus, M. Ritala, M. Leskelä, T. Prohaska, R. Resch, G. Friedbacher, and M. Grasserbauer, *AFM studies on ZnS thin films grown by atomic layer epitaxy*, Appl Surf Sci, 1997. **120**: p. 43-50.

25. S. Spiering, D. Hariskos, M. Powalla, N. Naghavi, and D. Lincot, *Cd-free Cu(In,Ga)Se2 thin film solar modules with In2S3 buffer layer by ALCVD*, Thin Solid Films, 2003. **431-432**: p. 359-363.

26. M. Bodegård, J. Kessler, O. Lundberg, J. Schöldström, and L. Stolt, *Growth of coevaporated Cu(In,Ga)Se2 - The influence of rate profiles on film morphology*. in *Proc. of the Materials Research Society Symposium*. 2001. San Fransisco, p. H2.2.1-12

27. R. Scheer, *Surface and interface properties of Cu-chalcopyrite semiconductors and devices*, Trends in Vacuum Science and Technology, 1997. **2**: p. 77-112.

28. D. Schmid, M. Ruckh, F. Grunwald, and H.W. Schock, *Chalcopyrite/defect chalcopyrite heterojunctions on the basis of CuInSe2*, J. Appl. Phys., 1993. **73**(6): p. 2902-2909.

29. M. Ruckh, D. Schmid, M. Kaiser, R. Schäffler, T. Walter, and H.W. Schock, *Influence of substrates on the electrical properties of Cu(In,Ga)Se2 thin films*. in *Proc. of the 1st World Conference on Photovoltaic Energy Conversion*. 1994. Hawaii, p. 156-159

30. L. Stolt, J. Hedström, and D. Sigurd, *Coevaporation with rate control system based on quadrupole mass spectrometer*, Journal of Vacuum Science and Technology, 1985. **3**: p. 403-407.

31. J. Kessler, C. Chityuttakan, J. Schöldström, and L. Stolt, *Growth of Cu(In,Ga)Se2 films using a Cu-poor/rich/poor sequence: substrate temperature effects*, Thin Solid Films, 2003. **431-432**: p. 1-5.

32. M. Edoff, S. Woldegiorgis, P. Neretnieks, M. Ruth, J. Kessler, and L. Stolt, *CIGS submodules with high performance and high manufacturability*. in *Proc. of the 19th European Photovoltaic Solar Energy Conference*. 2004. Paris, p. 1690-1693

33. J. Sterner, J. Kessler, M. Bodegård, and L. Stolt, *Atomic layer epitaxy growth of ZnO buffer layers in Cu(In,Ga)Se2 solar cells*. in *Proc. of the 2nd World Conference on photovoltaic energy conversion*. 1998. Vienna, Austria, p. 1145-1148

34. D. Briggs and M.P. Seah, *Practical surface analysis*. 2 ed. Vol. 1. 1990, Guildford: John Wiley & Sons Ltd.

35. J. Kessler, K. Velthaus, M. Ruckh, R. Laichinger, and H.W. Schock, *Chemical bath deposition of CdS on CuInSe2, etching effects and growth kinetics*. in *Proc. of the 6th international photovoltaic science and engineering conference*. 1992. New Delhi, India, p. 1005-1010

36. J.W. Elam and S.M. George, *Growth of ZnO/Al2O3 alloy films using atomic layer deposition techniques*, Chem. Mater., 2003. **15**: p. 1020-1028.

37. www.planar.com.

38. U. Özgur, Y. Alivov, C. Liu, A. Teke, M. Reshchikov, S. Dogan, V. Avrutin, S. Cho, and H. Morkoc, *A comprehensive review of ZnO materials and devices*, Journal of Applied Physics, 2005. **98**: p. 041301-103.

39. D. Lide, ed. *Handbook of chemistry and physics*. 2004-2005, CRC Press.

40. S.M. Sze, *Physics of semiconductor devices*. 1981, New York: John Wiley & Sons Inc.

41. M. Cardona, M. Weinstein, and G. Wolf, *Ultraviolet reflection spectrum of cubic CdS*, Physical Review, 1965. **140**(2A): p. 633-667.

42. A. Yamada, B. Sang, and M. Konagai, *Atomic layer deposition of ZnO transparent conducting oxides*, Appl Surf Sci, 1997. **112**: p. 216-222.

43. V. Lujala, J. Skarp, M. Tammenmaa, and T. Suntola, *Atomic layer epitaxy growth of doped zinc oxide thin films from organometals*, Appl Surf Sci, 1994. **82/83**: p. 34-40.

44. M. Tammenmaa, T. Koskinen, L. Hiltunen, and L. Niinistö, *Zinc calcogenide thin films grown by the atomic layer epitaxy technique using zinc acetate as source material*, Thin Solid Films, 1985. **124**: p. 125-128.

45. S. Kim, C. Hwang, S.-H. Park, and S. Yun, *Comparison between ZnO films grown by atomic layer deposition using H2O or O3 as oxidant*, Thin Solid Films, 2005. **478**: p. 103-108.

46. E. Yousfi, J. Fouache, and D. Lincot, *Study of atomic layer epitaxy of zinc oxide by in-situ quartz crystal microgravimetry*, Appl Surf Sci, 2000. **153**: p. 223-234.

47. S. Chaisitsak, T. Sugiyama, A. Yamada, and M. Konagai, *Cu(In,Ga)Se2 thin film solar cells with high resistivity ZnO buffer layers deposited by atomic layer deposition*, Jpn J Appl Phys, 1999. **38**: p. 4989-4992.

48. C. Liu, M. Yokoyama, Y. Su, and N. Lee, *Atomic Layer Epitaxy of ZnS by low-pressure horizontal metalorganic chemical vapor deposition*, Jpn. J. Appl. Phys., 1996. **35**: p. 2749-2753.

49. A. Hunter and A. Kitai, *A novel atmospheric pressure technique for the deposition of ZnS by atomic layer epitaxy using dimethylzinc*, J Cryst Growth, 1988. **91**: p. 111-118.

50. B.K. Meyer, A. Polity, B. Farangis, Y. He, D. Hasselkamp, T. Krämer, and C. Wang, *Structural properties and bandgap bowing of ZnO1-xSx thin films deposited by reactive sputtering*, Applied physics letters, 2004. **85**(21): p. 4929-4931.

51. B. Sanders and A. Kitai, *Zinc Oxysulfide thin films grown by atomic layer deposition*, Chem. Mater., 1992. **4**: p. 1005-1011.

52. S.N. Qui, C.X. Qui, and I. Shih, *CdZnSO and ZnSO films for optoelectronic application*, Can J Phys, 1989. **67**: p. 435-439.

53. A. Ohtomo, M. Kawasaki, T. Koida, K. Masubuchi, and H. Koinuma, *MgxZn1-xO as a II-VI widegap semiconductor alloy*, Applied physics letters, 1998. **72**(19): p. 2466-2468.

54. M. Putkonen, M. Nieminen, and L. Niinistö, *Magnesium aluminate thin films by atomic layer deposition from organometallic precursors and water*, Thin Solid Films, 2004. **466**: p. 103-107.

55. Y. Chiba, H. Miyazaki, A. Yamada, and M. Konagai, *MOCVD-Zn1-xMgxO as a novel buffer layer for Cu(In,Ga)Se2 solar cells*. in *Proc. of the 19th European Photovoltaic Solar Energy Conference*. 2004. Paris, France, p. 1737-1740

56. A. Fahrenbruch and R. Bube, *Fundamentals of solar cells: Photovoltaic solar energy conversion*. 1983, New York: Academic Press.

57. N. Ashcroft and D. Mermin, *Solid State Physics*. 1976, USA: Saunders College Publishing.

58. M. Cardona and L. Ley, eds. *Photoemission in Solids I General Principles*. 1978, Springer-Verlag: Berlin.

59. A. Zangwill, *Physics at surfaces*. 1988, Cambridge: Cambridge University Press.

60. S. Fonash, *Solar cell device physics*, ed. J. Denton. 1981, New York: Academic Press Inc.

61. J. Malmström, *On generation and recombination in Cu(In,Ga)Se2 thin-film solar cells*, PhD Thesis, *Faculty of Science and Technology*. 2005, Uppsala University: Uppsala.

62. U. Rau and H. Schock, *Electronic properties of Cu(In,Ga)Se2 heterojunction solar cells - recent achievements, current understanding and future challenges*, Appl Phys A, 1999. **69**: p. 131-147.

63. T. Wada, N. Kohara, S. Nishiwaki, and T. Negami, *Characterization of the Ci(In,Ga)Se2/Mo interface in CIGS solar cells*, Thin Solid Films, 2001. **387**: p. 118-122.

64. R. Klenk, *Characterisation and modelling of chalcopyrite solar cells*, Thin Solid Films, 2001. **387**: p. 135-140.

65. A. Niemegeers, M. Burgelman, and A.D. Vos, *On the CdS/CuInSe2 conduction band discontinuity*, Applied physics letters, 1995. **67**(6): p. 843-845.

66. G. Turner, R. Schwartz, and J. Gray, *Band discontinuity and bulk vs interface recombination in CdS/CuInSe2 solar cells*. in *Proc. of the 20th IEEE Photovoltaics Specialists Conference*. 1988. Las Vegas, p. 1457-1460

67. M. Burgelman, P. Nollet, and S. Degrave, *Modelling polycrystalline semiconductor solar cells*, Thin Solid Films, 2000. **361-362**: p. 527-532.

68. I. Eisgruber, J. Granata, J.R. Sites, J. Hou, and J. Kessler, *Blue-photon modification of nonstandard diode barrier in CuInSe2 solar cells*, Solar Energy Materials and Solar Cells, 1998. **53**: p. 367-377.

69. A. Niemegeers, M. Burgelman, R. Herberholz, U. Rau, D. Hariskos, and H.W. Schock, *Model for electronic transport in Cu(In,Ga)Se2 solar cells*, Progress in Photovoltaics: Research and application, 1998. **6**: p. 407-421.

70. R. Herberholz, U. Rau, H.W. Schock, T. Haalboom, T. Gödecke, F. Ernst, C. Beilharz, K.W. Benz, and D. Cahen, *Phase segregation, Cu migration and junction formation in Cu(In,Ga)Se2*, The European Physical Journal, Applied Physics, 1999. **6**: p. 131-139.

71. M. Igalson, M. Bodegård, L. Stolt, and A. Jasenek, *The defected layer and the mechanism of the interface-related metastable behavior in the ZnO/CdS/Cu(In,Ga)Se2 devices*, Thin Solid Films, 2003. **431-432**: p. 153-157.

72. M. Igalson and C. Platzer-Björkman, *The influence of buffer layer on the transient behaviour of thin film chalcopiryte devices*, Solar Energy Materials and Solar Cells, 2004. **84**: p. 93-103.

73. Q. Nguyen, K. Orgassa, I. Koetschau, U. Rau, and H.W. Schock, *Influence of heterointerfaces on the performance of Cu(In,Ga)Se2 solar cells with CdS and In(OHx,Sy) buffer layers*, Thin Solid Films, 2003. **431-432**: p. 330-334.

74. A.D. Katani and G. Margaritondo, *Microscopic study of semiconductor heterojunctions: Photoemission measurement of the valence-band discontinuity and of the potential barriers*, Physical Review B, 1983. **28**(4): p. 1944-1956.

75. J. Sterner, J. Kessler, and L. Stolt, *XPS instrument coupled with ALCVD reactor for investigation of film growth*, J Vac Sci Technol A, 2002. **20**(1): p. 278-284.

76. G. Venkata Rao, F. Säuberlich, and A. Klein, *Influence of Mg content on the band alignment at CdS/(Zn,Mg)O interfaces*, Applied physics letters, 2005. **87**: p. 032101.

77. T. Minemoto, Y. Hashimoto, T. Satoh, T. Negami, H. Takakura, and Y. Hamakawa, *Cu(In,Ga)Se2 solar cells with controlled conduction band offset of window/Cu(In,Ga)Se2 layers*, J Appl Phys, 2001. **89**(12): p. 8327-8330.

78. U. Malm, Determination of dominant recombination mechanisms in Cu(In,Ga)Se2 thin film solar cells with ALD-ZnO buffer layers, Master Thesis, Uppsala University, 2003

79. K. Orgassa, U. Rau, Q. Nguyen, H.W. Schock, and J. Werner, *Role of the CdS Buffer layer as an active optical element in Cu(In,Ga)Se2 thin-film solar cells*, Progress in Photovoltaics: Research and application, 2002. **10**: p. 457-463.

80. U. Malm, J. Malmström, C. Platzer-Björkman, and L. Stolt, *Determination of dominating recombination paths in Cu(In,Ga)Se2 thin film solar cells with ALD-ZnO buffer layers*, Thin Solid Films, 2005. **480-481**: p. 208-212.

81. P. Zabierowski, U. Rau, and M. Igalson, *Classification of metastabilities in the electrical characteristics of ZnO/CdS/Cu(In,Ga)Se2 solar cells*, Thin Solid Films, 2001. **387**: p. 147-150.

82. U. Rau, K. Weinert, Q. Nguyen, M. Mamor, G. Hanna, A. Jasenek, and H.W. Schock, *Device analysis of Cu(In,Ga)Se2 heterojunction solar cells - some open questions*. in *Proc. of the Materials Research Society Symposium*. 2001. San Fransisco, p. H9.1.1-12

83. U. Rau, D. Braunger, R. Herberholz, H. Schock, J. Guillemoles, L. Kronik, and D. Cahen, *Oxygenation and air-annealing effects on the electronic properties of Cu(In,Ga)Se2 films and devices*, J Appl Phys, 1999. **86**(1): p. 497-505.

84. U. Malm and L. Stolt, *Long term stability in Cu(In,Ga)Se2 solar cells with different buffer materials*. To appear in *Proc. of the 20th European Photovoltaic Solar Energy Conference*, 2005, Barcelona

85. M. Contreras, H. Wiesner, D. Niles, K. Ramanathan, R. Matson, J. Tuttle, J. Keane, and R. Noufi, *Defect chalcopyrite Cu(In1-xGax)3Se5 materials and high-Ga-content Cu(In,Ga)Se2 based solar cells*. in *Proc. of the 25th IEEE Photovoltaic Specialists Conference*. 1996. Washington D.C., p. 809-812

86. D. Cahen and R. Noufi, *Defect chemical explanation for the effect of air anneal on CdS/CuInSe2 solar cell performance*, Applied physics letters, 1989. **54**: p. 558-560.

87. R. Herberholz, M. Igalson, and H.W. Schock, *Distinction between bulk and interface states in CuInSe2/CdS/ZnO by space charge spectroscopy*, Journal of Applied Physics, 1997. **83**(1): p. 318-325.

88. C.-S. Jiang, F.S. Hasoon, H.R. Moutinho, H.A. Al-Thani, M. Romero, and M. Al-Jassim, *Direct evidence of a buried homojunction in Cu(In,Ga)Se2 solar cells*, Applied physics letters, 2003. **82**(1): p. 127-129.

89. K. Ramanathan, R. Bhattacharya, J. Granata, J. Webb, D. Niles, M. Contreras, H. Wiesner, F. Hasoon, and R. Noufi, *Advances in the CIS research at NREL*. in *Proc. of the 26th IEEE Photovoltaics Specialists Conference*. 1997. Anaheim, Canada, p. 319-322

90. K. Ramanathan, H. Wiesner, S. Asher, D. Niles, R. Bhattacharya, J. Keane, M. Contreras, and R. Noufi, *High efficiency Cu(In,Ga)Se2 thin film solar cells without intermediate buffer layers*. in *Proc. of the 2nd World Conference on Photovoltaic Energy Conversion*. 1998. Vienna, Austria, p. 477-481

91. T. Nakada and A. Kunioka, *Direct evidence of Cd diffusion into Cu(In,Ga)Se2 thin films during chemical-bath deposition process of CdS films*, Appl. Phys. Lett., 1999. **74**(17): p. 2444-2446.

92. T. Nakada, *Diffusion behaviour and microstructural properties of the CBD-ZnS/CIGS interface boundary*. in *Proc. of the Materials Research Society Symposium*. 2001. San Fransisco, p. H7.1.1-9

93. T. Sugiyama, S. Chaisitsak, A. Yamada, M. Konagai, Y. Kudriavtsev, A. Godines, A. Villegas, and R. Asomoza, *Formation of pn homojunction in Cu(In,Ga)Se2 thin film solar cells by Zn doping*, Jpn J Appl Phys, 2000. **39**: p. 4816-4819.

94. T.M. Friedlmeier, D. Braunger, D. Hariskos, M. Kaiser, H.N. Wanka, and H.W. Schock, *Nucleation and growth of the CdS buffer layer on Cu(In,Ga)Se2 thin films*. in *Proc. of the 25th IEEE Photovoltaic Specialists Conference*. 1996. Washington, p. 845-848

95. L. Weinhardt, M. Bär, H. Muffler, C. Fisher, M. Lux-Steiner, T. Niesen, F. Karg, T. Gleim, C. Heske, and E. Umbach, *Impact of Cd2+ treatment on the band alignment at the ILGAR-ZnO/CuIn(S,Se)2 heterojunction*, Thin Solid Films, 2003. **431-432**: p. 272-276.

96. S. Wei and A. Zunger, *Band offsets and optical bowings of chalcopyrites and Zn-based II-VI alloys*, Journal of Applied Physics, 1995. **78**: p. 3846-3856.

97. M. Turcu and U. Rau, *Compositional trends of defect energies, band alignments, and recombination mechanisms in the Cu(In,Ga)(S,Se)2 alloy system*, Thin Solid Films, 2003. **431-432**: p. 158-162.

98. U. Rau, M. Schmitt, D. Hilburger, F. Engelhardt, O. Seifert, and J. Parisi, *Influence of Na and S incorporation on the electronic transport properties of Cu(In,Ga)Se2 solar cells*. in *Proc. of the 25th IEEE Photovoltaics Specialists Conference*. 1996. Washington D. C., p. 1005-1008

99. K. Kushiya, S. Kuriyagawa, T. Kase, M. Tachiyuki, I. Sugiyama, Y. Satoh, M. Satoh, and H. Takeshita, *The role of Cu(In,Ga)(Se,S)2 surface layer on a graded band-gap Cu(In,Ga)Se2 thin-film solar cell prepared by two-stage method*. in *Proc. of the 25th IEEE Photovoltaics Specialists Conference*. 1996. Washington D C, p. 989-992

100. J. Palm, V. Probst, and F. Karg, *Second generation CIS solar modules*, Solar Energy, 2004. **77**: p. 757-765.

101. Y. Nagoya, K. Kushiya, M. Tachiyuki, and O. Yamase, *Role of incorporated sulfur into the surface of Cu(In,Ga)Se2 thin film absorber*, Solar Energy Materials & Solar Cells, 2001. **67**: p. 247-253.

102. T. Nakada, H. Ohbo, T. Watanabe, H. Nakazawa, M. Matsui, and A. Kunioka, *Improved Cu(In,Ga)(S,Se)2 thin film solar cells by surface sulfurization*, Solar Energy Materials & Solar Cells, 1997. **49**: p. 285-290.

103. T. Nakada, K. Matsumoto, and M. Okumura, *Improved efficiency of Cu(In,Ga)Se2 thin film solar cells by surface sulfurization using wet process*. in *Proc. of the 29th IEEE Photovoltaics Specialists Conference*. 2002. New Orleans, p. 527-530

104. J. Sterner, *ALD buffer layer growth and interface formation on Cu(In,Ga)Se2 solar cell absorbers*, PhD Thesis, *Department of engineering science*. 2004, Uppsala University: Uppsala.

105. J. Keränen, J. Lu, J. Barnard, J. Sterner, J. Kessler, L. Stolt, T. Matthes, and E. Olsson, *Effect of sulfurization on the microstructure of chalcopyrite thin-film absorbers*, Thin Solid Films, 2001. **387**: p. 80-82.

106. J. Sterner, T. Matthes, J. Kessler, J. Lu, J. Keränen, E. Olsson, and L. Stolt, *Sulfurization of thin film solar cell absorbers*. in *Proc. of the 16th European Photovoltaic Solar Energy Conference*. 2000. Glasgow, UK, p. 771-774

107. R. Menner, B. Dimmler, R. Mauch, and H.W. Schock, *II-VI compound thin films for windows in heterojunction solar cells*, JOurnal of crystal growth, 1988. **86**: p. 906-911.

108. V. Nadenau, D. Hariskos, H.W. Schock, M. Krejci, F.J. Haug, A. Tiwari, H. Zogg, and G. Kostorz, *Microstructural study of the CdS/CuGaSe2 interfacial region in CuGaSe2 thin film solar cells*, J Appl Phys, 1999. **85**(1): p. 534-542.

109. D. Abou-Ras, D. Rudmann, G. Kostorz, S. Spiering, M. Powalla, and A. Tiwari, *Microstructural and chemical studies of interfaces between Cu(In,Ga)Se2 and In2S3 layers*, Journal of Applied Physics, 2005. **97**: p. 084908-1-8.

Acta Universitatis Upsaliensis

Digital Comprehensive Summaries of Uppsala Dissertations from the Faculty of Science and Technology 136

Editor: The Dean of the Faculty of Science and Technology

A doctoral dissertation from the Faculty of Science and Technology, Uppsala University, is usually a summary of a number of papers. A few copies of the complete dissertation are kept at major Swedish research libraries, while the summary alone is distributed internationally through the series Digital Comprehensive Summaries of Uppsala Dissertations from the Faculty of Science and Technology. (Prior to January, 2005, the series was published under the title "Comprehensive Summaries of Uppsala Dissertations from the Faculty of Science and Technology".)

Distribution: publications.uu.se
urn:nbn:se:uu:diva-6263

ACTA
UNIVERSITATIS
UPSALIENSIS
UPPSALA
2006